On the interplay between roughness and viscoelasticity in adhesive hysteresis

Pérez-Ràfols, Francesc; Van Dokkum, Jan Steven; Nicola, Lucia

DOI
10.1016/j.jmps.2022.105079

Publication date
2023

Document Version
Final published version

Published in
Journal of the Mechanics and Physics of Solids

J. Mech. Phys. Solids 170 (2023) 105079

Contents lists available at ScienceDirect

Journal of the Mechanics and Physics of Solids

journal homepage: www.elsevier.com/locate/jmps

On the interplay between roughness and viscoelasticity in adhesive hysteresis

Francesc Pérez-Ràfols [a,b], Jan Steven Van Dokkum [c], Lucia Nicola [a,c,*]

[a] Department of Industrial Engineering, University of Padova, 35131 Padua, Italy
[b] Serra Hunter Fellow at the Department of Mining, Industrial & ICT Engineering (Industrial Technologies), E.P.S.E. Manresa, Universitat Politécnica de Catalunya (UPC), Barcelona, Spain
[c] Department of Materials Science and Engineering, Delft University of Technology, 2628CD Delft, The Netherlands

ARTICLE INFO

Keywords:
Adhesion and adhesives
Contact mechanics
Viscoelastic material
Adhesive hysteresis

ABSTRACT

Viscoelasticity and roughness are among the possible causes of the adhesive hysteresis displayed by soft contacts. Viscoelasticity causes an increased effective work of adhesion due to stiffening of the contact, while roughness is responsible for elastic instabilities. Herein, we explore the interplay between viscoelasticity and roughness by simulating in two dimensions the retraction of a rigid cylinder, with wavy surface profile, from a viscoelastic half-space. The wave amplitude and length are varied to induce instabilities in the load–to–area response, while the retraction velocity is increased to promote viscoelasticity. Results show that, in the regime where viscoelasticity is confined to the edges of the wavy contact, the contributions of viscoelasticity and waviness to adhesive hysteresis are nearly independent and additive. At low retraction rates, the instabilities in the load-area curve typical of rough elastic contacts are suppressed by viscoelasticity: the contact stiffens to promote a stable decrease of the contact area with load. This occurs with a minimal change in work of adhesion. However, when the instantaneous limit is met at high retraction rates, mechanical instabilities appear.

1. Introduction

Soft material adhesive contact occurs in a large variety of engineering applications that include automotives (Tiwari et al., 2021); aerospace (Chizhik et al., 2020); nano-engineering (Neupane et al., 2021); robotics (Coulson et al., 2022); bio-medics (Jeong et al., 2015); and, bio-engineering (Mazzotta et al., 2020). A critical aspect of soft contacts is that they display adhesive hysteresis, i.e., contact deformation is mechanically reversible, yet energetically irreversible. Adhesive hysteresis is commonly observed as a larger intimate contact area during normal retraction, than during indentation. Predicting and controlling adhesive hysteresis is paramount in the design, and for the operation of the aforementioned engineering applications. However the origins as well as the physical mechanisms behind adhesive hysteresis in rough adhesive contacts are at present ill understood (Johnson, 2000; Lin and Hui, 2002; Lorenz et al., 2013; Popov, 2021; Papangelo and Ciavarella, 2021b). The sources of adhesive hysteresis in soft contacts are numerous and intertwined, and include viscoelasticity (Lorenz et al., 2013; Tiwari et al., 2017), elastic instabilities (Guduru, 2007; Zhu et al., 2021), chemical irreversibility related to the formation and destruction of bonds at the contacting surfaces (Chen et al., 1991; Chaudhury et al., 1996), and surface roughness (Carbone et al., 2015; Dalvi et al., 2019). Herein, we will neglect chemistry and focus on mechanics only. More specifically, we aim to elucidate the effect of roughness on adhesive viscoelastic hysteresis, as it is still unclear (Kesari et al., 2010; Baek et al., 2017; Greenwood, 2017; Dorogin et al., 2017; Deng and Kesari, 2019).

* Corresponding author at: Department of Materials Science and Engineering, Delft University of Technology, 2628CD Delft, The Netherlands.
E-mail address: lucia.nicola@unipd.it (L. Nicola).

https://doi.org/10.1016/j.jmps.2022.105079
Received 9 June 2022; Received in revised form 30 August 2022; Accepted 17 September 2022
Available online 22 September 2022

Adhesion causes energetically irreversible mechanical behaviour even when contact is smooth and elastic: the load–displacement curve obtained during indentation differs from the one obtained upon retraction (Ciavarella et al., 2017, 2019; Wang et al., 2021), as the jump–in and –out of contact occur at different loads. This implies that energy is dissipated during the indentation–retraction cycle. When the contact is rough, the elastic response and hysteresis change (Ciavarella et al., 2017). Guduru (2007) showed that in wavy, elastic contacts the equilibrium load–area curve is characterized by oscillations that lead to unstable elastic jumps. These jumps occur at larger loads during indentation than during retraction. As a result, adhesion increases upon separation of the surfaces, and the pull-off load is larger than in smooth contact (Guduru, 2007), i.e. one finds additional roughness–induced dissipation. The theory proposed by Guduru is limited to contact with a simply connected contact area, and is validated experimentally by Guduru and Bull (2007) and numerically by Carbone et al. (2015). Kesari and Lew (2011) extended Guduru's theory (Guduru, 2007) to include general contact roughness, and predicted hysteresis in agreement with the experimental results by Kesari et al. (2010). Evidence that small–scale roughness enhances the pull–off load is provided as well in Fuller and Tabor (1975), Briggs and Briscoe (1977), Fuller and Roberts (1981), and justified by Persson and Tosatti (2001) who attributed it to the increase in surface area and therefore intimate contact area between realistic rough surfaces. The theories on elastic rough contacts often show some disagreement with experimental observations. This is generally attributed to the presence of viscoelastic effects in experiments (Greenwood and Johnson, 1981; Chaudhury et al., 1996; Vaenkatesan et al., 2006; Lorenz et al., 2013; Tiwari et al., 2017; Violano and Afferrante, 2019; Violano et al., 2022). A characteristic that distinguishes hysteresis due to viscous loss from hysteresis due to surface roughness is that the former is rate–dependent (Waters and Guduru, 2010).

Viscous dissipation plays a significant role even when the indentation and retraction rates are small compared to the material characteristic frequencies, as experimentally verified by Chaudhury et al. (1996), Lorenz et al. (2013), Tiwari et al. (2017), and Violano and Afferrante (2019), and later inferred theoretically by Papangelo and Ciavarella (2021b). The time–dependent behaviour for slow retraction is due to a high stress rate near the edges of intimate contact, which are therefore often treated as opening cracks (Gent and Petrich, 1969; Gent, 1971; Gent and Schultz, 1972). Recent numerical analyses (Van Dokkum et al., 2021; Afferrante and Violano, 2022; Müser and Persson, 2022) have confirmed that the predictions of the models by Greenwood (Greenwood, 2004) and Persson and Brener (Persson and Brener, 2005), based on crack propagation analyses, are accurate. It is customary to treat the increased adhesion caused by viscosity as an effective work of adhesion that increases with crack–tip velocity. The crack–tip analyses (Gent and Petrich, 1969; Gent, 1971; Gent and Schultz, 1972; Greenwood, 2004; Persson and Brener, 2005) are correct provided that retraction rates are lower than or close to the materials characteristic frequencies (Van Dokkum et al., 2021; Afferrante and Violano, 2022).

Very recently, much attention was dedicated to the study of the pull-off load in smooth, adhesive viscoelastic contacts (Violano and Afferrante, 2022a; Das and Chasiotis, 2021; Ciavarella, 2021b; Jiang et al., 2021), as pull-off is a measure of dissipation. When short-ranged adhesion is considered, the Gent and Schultz assumption (Gent and Petrich, 1969; Gent, 1971; Gent and Schultz, 1972) holds, i.e. viscous dissipation is confined to the edges of contact (Afferrante and Violano, 2022). However, viscoelastic stiffening tends to promote long-ranged adhesive behaviour as shown by Ciavarella (2021b), Van Dokkum et al. (2021), Müser and Persson (2022), and Violano and Afferrante (2022a). This readily rationalizes by considering that the Maugis parameter, which is typically used to assess whether an adhesive elastic contact is long– or short–ranged, depends on the elastic modulus. In a viscoelastic contact, the Maugis parameter is thus not a constant but a variable that decreases while the modulus departs from the relaxed limit (Van Dokkum et al., 2021). When the instantaneous limit is approached adhesion stops being short-ranged and departs from JKR–theory (Johnson et al., 1971). Müser and Persson (2022) show that when smooth cylinders are retracted at high rates dissipation is not limited to the contact edges, and with a decrease in radius and an increase in instantaneous moduli, the jump–out of contact transitions from crack–propagation to "*quasi–uniform*" bond breaking. Afferrante and Violano (2022), and Violano and Afferrante (2022a) find through a finite element analysis that marked viscous dissipation in the bulk of the material occurs when unloading from an "*unrelaxed*" state or when adhesion is long-ranged. According to their results (Afferrante and Violano, 2022; Violano and Afferrante, 2022a,b), the upper bound of the pull-off load depends on the Maugis parameter (Ciavarella, 2021b).

Despite the assumption by Gent and Petrich (1969), Gent (1971), and Gent and Schultz (1972) can break down for high retraction rates, it is at the basis of various studies on non–smooth viscoelastic adhesive contacts, that include wavy (Ciavarella and Papangelo, 2021), patterned (Papangelo and Ciavarella, 2021a) and multi–asperity (Violano et al., 2021b,c) roughness. The results indicate that, in the presence of viscoelasticity (Violano et al., 2021b,c) at low retraction rates, roughness increases the pull–off load (negligibly according to some authors (Violano et al., 2021b,c), significantly according to others (Papangelo and Ciavarella, 2021a; Ciavarella and Papangelo, 2021)). Whether this happens at high retraction rates as well, is more controversial (Ciavarella and Papangelo, 2021; Papangelo and Ciavarella, 2021a). Similarly, it is still unknown how surface roughness affects the dependence of the pull–off load on the maximum applied load (Violano et al., 2021c).

Herein, we aim at contributing to a better understanding of the interplay between roughness, viscoelasticity and adhesion by means of a simple two–dimensional numerical model, which has the strength that the rate-dependent dissipation is an emergent behaviour. As such, no assumption is made on whether adhesion is short or long–ranged. The model builds on the work by Van Dokkum and Nicola (2019), and Van Dokkum et al. (2021), who study the indentation and retraction of a smooth, rigid cylinder from a viscoelastic half-plane by means of Green's function molecular dynamics (Prodanov et al., 2014). To simplify the problem, roughness is modelled as a single wave superimposed on the profile of a rigid cylinder retracting from the viscoelastic half–plane. By changing retraction speed from different initial loads, we track the contact area and compute the pull–off load for various wave amplitudes and lengths. Also, by contrasting elastic and viscoelastic simulations we verify an interesting speculation recently made by Papangelo and Ciavarella (2021a) and Ciavarella and Papangelo (2021), namely that viscoelasticity "effectively dampens" (Ciavarella and Papangelo, 2021) the roughness–induced elastic instabilities.

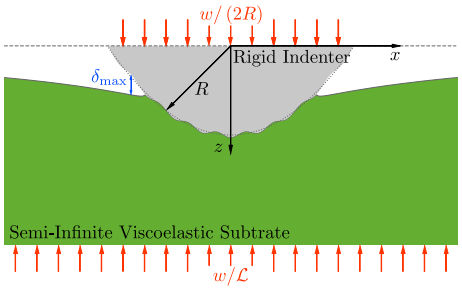

Fig. 1. A rigid indenter with radius R in contact with a viscoelastic substrate for an applied load w. Adhesion is controlled by the interaction length $\delta_{\max}$. The image is stretched in the z–direction for clarity.

2. Problem definition

The problem considered in this work is the retraction of a rigid, wavy, infinitely long, cylindrical indenter from a viscoelastic half–plane, as represented schematically in Fig. 1. First, we indent the substrate elastically, with the relaxed effective modulus E_0^*, up to a maximum load $w_{\max}$. This is equivalent to indenting a viscoelastic substrate and prescribing an infinite waiting time, so the substrate fully relaxes after indentation, but computationally tractable. Subsequently, the indenter is retracted by reducing the load at a constant rate $\dot{w}$, where the overdot $\dot{\bullet}$ indicates the derivative of $\bullet$ with respect to the dimensional time t.

The cylindrical indenter, which is assumed to be much stiffer than the substrate, has a profile

$$h(x,t) = h_0(t) + \frac{x^2}{2R} - A\cos\left(\frac{2\pi x}{\zeta}\right), \tag{1}$$

where the first term characterizes a rigid body translation, the second the profile of a Hertzian cylinder with radius R and the third a sinusoidal waviness, superimposed on the cylindrical profile, with amplitude A and wavelength ζ. As shown in Fig. 1, the phase of the wave is chosen such that a minimum resides at the centre of the contact (i.e., at the position $x = 0$). A phase shift changes the contact mechanical response (Waters et al., 2009), however, herein we do not explore the effects of such changes.

The substrate is assumed to be initially flat and semi–infinite. The material is taken to be incompressible (with a Poisson's ratio $\nu = 1/2$) and viscoelastic in shear. As in all contact mechanics problems, the effective modulus is given by $E^* = 2\mu/(1-\nu^2)$, where μ is the shear modulus. For simplicity, the viscoelastic behaviour is modelled by means of the Zener model (Marques and Creus, 2012). Hence, the creep function of the equivalent elastic modulus is

$$E^*(t) = E_0^* + \left(E_\infty^* - E_0^*\right) e^{-\frac{t}{\tau}}, \tag{2}$$

where E_0^* is the relaxed effective modulus, that characterizes the response when the deformation rate $\dot{u} \sim 0$; E_∞^* the instantaneous effective modulus, that characterizes the response in the limit $\dot{u} \to \infty$; and, τ the relaxation time. It should be noted that the literature is not consistent with their definition and in some other works, e.g. Greenwood and Johnson (1981), E_∞ denotes the relaxed modulus and E_0 the instantaneous one. Moreover, the terms adiabatic and glassy are used to indicate the relaxed and instantaneous states, particularly in the materials sciences literature.

The Dugdale–Maugis model (Dugdale, 1960; Maugis, 1992) is used to describe the adhesive interaction between the indenter and the (visco)elastic substrate. This model (Dugdale, 1960; Maugis, 1992) specifies an adhesive traction σ_a whenever the gap between the two bodies, $g(x,t)$, is positive but smaller than or equal to the interaction length $\delta_{\max}$. This leads to a work of adhesion $\Delta\gamma_0 = \sigma_a\delta_{\max}$. For elastic cases, it has been shown that the choice of the adhesion model has marginal effects on the results, e.g. Müser (2014). Viscoelastic materials are potentially more sensitive to this choice. Here, we select the simplest adhesion model, and leave for future investigation the effect that specific adhesion models might have on the results. Interpenetration is prevented through a hard-wall constraint. In summary, the following conditions describe the interfacial interaction:

$$\begin{aligned} g(x,t) = 0, &\quad p(x,t) < \sigma_a, &&\text{intimate contact;}\\ 0 < g(x,t) \le \delta_{\max}, &\quad p(x,t) = \sigma_a, &&\text{adhesive zone;}\\ g(x,t) > \delta_{\max}, &\quad p(x,t) = 0, &&\text{out of contact,} \end{aligned} \tag{3a}$$

with the gap

$$g(x,t) = h(x,t) - u(x,t), \tag{3b}$$

where $u(x,t)$ indicates the displacements of the (visco)elastic substrate. The normal pressure at the interface is indicated by $p(x,t)$. By convention, pressure is defined positive when compressive. The contact area a_c is defined as the area in intimate contact where the gap $g(x,t) = 0$.

The problem is studied by controlling the load rate $\dot{w}(t) = \frac{\partial}{\partial t}\int p(x,t)\,\mathrm{d}x$ at the contact and the rigid body movement ($h_0(t)$) is an output.

Herein, we focus mostly on short-ranged adhesion, for which the JKR theory applies (Johnson and Greenwood, 2008). This is a common choice, considering that experimental evidence shows that the JKR theory applies to many rubbery materials (Chaudhury et al., 1996; Baney and Hui, 1997; Waters and Guduru, 2010; Lorenz et al., 2013; Tiwari et al., 2017). Moreover, this choice ensures that our results compare with the analytical work by Guduru (2007). Short-ranged adhesion is achieved by selecting large values for the relaxed Maugis parameter, $\lambda_0 = \Delta\gamma_0 \left(R/E_0^{*2}\Delta\gamma_0 \right)^{1/3}/\delta_{\max}$, as we show in the following. Also, herein, we limit our attention to small length–scale roughness to ensure that the small–slope approximation holds. Finally, we restrict the analysis to a slow retraction rate with the aim of concentrating viscous dissipation near the edges of contact. This regime is studied intensively in recent times both experimentally by Waters and Guduru (2010), Lorenz et al. (2013), Tiwari et al. (2017), Ciavarella and Papangelo (2021) and analytically by Ciavarella (2021a,b). We emphasize, however, that the model is applicable to long–ranged adhesion and high retraction rates as well.

3. Numerical method

The numerical model adopted is the one presented by Van Dokkum and Nicola (2019), which employs the Green's Function Molecular Dynamics (GFMD) technique and discrete Fourier transform to achieve an efficient algorithm. The GFMD technique is a boundary–element method that permits one to reduce the dimensionality of the problem such that only the profile of the substrate is explicitly discretized and modelled. At each temporal increment of the retraction of the cylinder, the equilibrium normal displacement of the profile is found by means of the following relation in Fourier space:

$$\tilde{p}\,(q,t) + \tau\dot{\tilde{p}}\,(q,t) = -8|q|\left(E_0^*\tilde{u}\,(q,t) + \tau E_\infty^*\dot{\tilde{u}}\,(q,t)\right), \tag{4}$$

coupled to the imposed boundary conditions. Here, the overscript tilde $\tilde{\bullet}$ indicates the Fourier transform of $\bullet$, with the wavenumber q. The procedure to derive Eq. (4) is presented in Van Dokkum and Nicola (2019) and involves solving first the elastic problem and then using the correspondence principle to translate the results to the viscoelastic case. Finally, the resulting equation is particularized to the Zener model described by the equivalent elastic modulus given in Eq. (2). The reader is referred to Van Dokkum and Nicola (2019) for further details. The only modification made with respect to the model presented in Van Dokkum and Nicola (2019) is that adhesion is here implemented using a first–order approximation in the gap, in a manner similar to that presented by Medina and Dini (2014).

As shown in Van Dokkum and Nicola (2019), Eq. (4) is integrated in the time domain semi–analytically within each constant, dimensional time–step Δt. We thus avoid storing the whole history of normal pressures and displacement, which is necessary for a direct numerical integration. Each dimensionless time–step $\Delta\bar{t}$, the position (Störmer–)Verlet algorithm (Störmer, 1912) is used to compute, through damped dynamics, the new normal displacement of the equispaced nodes n_x that discretize the profiles. The periodic width $10R \leq \mathcal{L}$. The pseudo–code of the algorithm is given in Appendix A. The convergence analysis is performed for both the spatial and temporal discretizations, n_x and Δt, respectively, and the results are provided in Appendix B.

We note that the relation between normal pressure p and displacement u, given in Eq. (4), becomes degenerate at the centre–of–mass mode, $q = 0$. This well–known issue in two-dimensional contact mechanics makes the centre–of–mass displacement, $\tilde{u}\,(q=0)$, undefined (see Johnson, 1985). Hence, the approach between the two surfaces cannot be trivially defined and is not used in the following.

4. Wavy elastic contacts

We first consider the retraction of a wavy, adhesive, infinitely long cylinder from an elastic half–plane, which serves as a means of comparison for the retraction from a viscoelastic substrate. Herein, we include as reference also the analytical solution to the same problem as presented by Guduru (2007). He provides a relation between the contact area a_c and the load w for short–ranged adhesion. This relation, expressed in terms of the dimensionless variables presented in Appendix C, reads

$$\bar{w} = \frac{\pi}{4}\bar{a}_c^2 - \sqrt{2\pi\bar{a}_c} + \pi\alpha\bar{a}_c \mathrm{J}_1\left(\frac{2\pi\bar{a}_c}{\beta}\right), \tag{5a}$$

with the normalized amplitude and wavelength,

$$\alpha = \frac{\pi A E^*}{\zeta}\left(\frac{R}{(E^*)^2\,\Delta\gamma}\right)^{1/3}; \qquad \text{and,} \qquad \beta = \zeta\left(\frac{E^*}{R^2\Delta\gamma}\right)^{1/3}, \tag{5b}$$

respectively, where J_1 is the first Bessel function of order one. The first two terms on the right-hand side of Eq. (5a) correspond with the two-dimensional JKR solution (see e.g. Chaudhury et al., 1996; Johnson and Greenwood, 2008) and the third one incorporates the effect of waviness. The normalized amplitude α and normalized wavelength β are measures of the amplitude and frequency of the load–area oscillations. Note that, while β is also the normalized wavelength of the waviness, its dimensionless amplitude is $\alpha/(\pi\beta)$. Guduru's original solution expresses this third term through an infinite sum, that we evaluate. Also, herein, we use different dimensionless parameters than those presented in Guduru (2007), to include the length scale of the adhesive interaction $\delta_{\max}$. The term $\pi A E^*/\zeta$ in the normalized amplitude α corresponds to the pressure amplitude that results from flattening a wave with amplitude A and wavelength ζ (Johnson et al., 1985), and is multiplied with a cubed–root term that considers adhesion. The load–area curves defined by Eq. (5) are shown in Fig. 2 with dotted lines for the normalized amplitudes $\alpha = 0,\ 0.37,\ 1.46$ and 5.87 in Fig. 2(a), and normalized wavelengths $\beta = 0,\ 0.47,\ 1.87$ and ∞ in Fig. 2(b); the maximum normalized load is

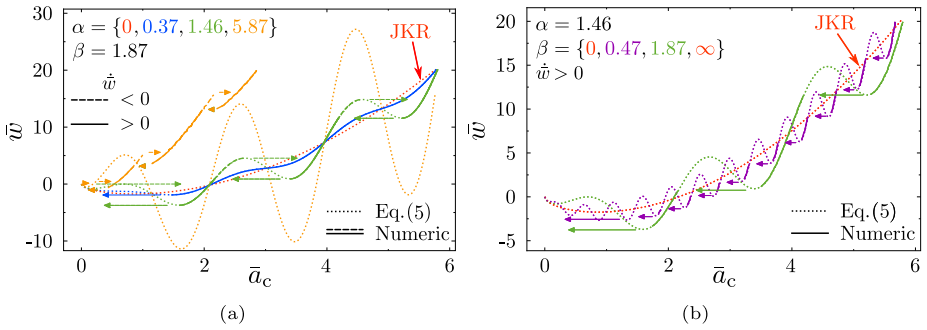

Fig. 2. Load-Area curves for (a) the normalized amplitudes $\alpha = 0$, 0.37, 1.46 and 5.87, and (b) the normalized wavelengths $\beta = 0$, 0.47, 1.87 and ∞. The maximum normalized load $\bar{w}_{\max} = 20$. The dotted lines indicate Guduru's solution (5), the dashed and solid lines the numerical results for indentation ($\dot{\bar{w}} < 0$) and retraction ($0 < \dot{\bar{w}}$), respectively, and the arrows indicate unstable jumps.

$\bar{w}_{\max} = w_{\max}/\left(RE_0^*\Delta\gamma_0^2\right)^{1/3} = 20$. In Fig. 2(a), both indentation (dashed lines) and retraction paths (solid lines) are shown; in Fig. 2(b), only the retraction paths are presented. In the limiting case of $\alpha \sim 0$, the ball is smooth and the JKR-solution, indicated by the dotted red line in Fig. 2, is recovered.

In Fig. 2(a), the analytical curves are contrasted to the numerical results, indicated by solid and dashed lines and obtained using the method in Section 3. For low values of normalized amplitude $\alpha = 0.37$ (blue lines), the load-area response oscillates only slightly around the JKR–solution. As the normalized amplitude α increases to 1.46 (green dotted, solid and dashed lines), negative load–area slopes appear on the analytical curves (green and orange dotted lines). Guduru's solution (5) gives all static equilibrium positions. However, the trajectories with negative slope are unstable and hence inaccessible to the numerical solution and can neither be reached by a real system. Once a given local minimum in load is reached during retraction, an unstable jump occurs, as indicated by arrows that connect two stable static equilibria. During indentation, these jumps occur when the load reaches a local maximum. In this way, waviness leads to additional hysteresis, provided that the normalized amplitude α is large enough. Eventually, when the normalized amplitude $\alpha = 5.87$ (orange lines), the numerical solution deviates completely from Guduru's analytical solution. This is because Guduru's analysis assumes that the contact area is simply connected. At large normalized amplitudes, however, this assumption is violated as the contact only occurs at the minima of the waviness. Hence, Guduru's solution is no longer applicable.

In Fig. 2(b), the load–area curves during retraction are presented for the normalized wavelengths $\beta = 0.47$ and 1.87. As expected, the role of the normalized parameter β is to change the wavelength of the load–area oscillations and thus to change the frequency of the unstable jumps. These become sparser with increased normalized wavelength β. In particular, instabilities disappear when $\beta \sim 0$ because the contact is smooth. Also, in the limit $\beta \to \infty$, the elastic jumps are so numerous and short that a response that resembles a smooth contact is recovered.

Guduru's solution is valid in the case of short–ranged adhesion. When considering smooth cylinders, the relaxed Maugis parameter λ_0 is used to distinguish between short– and long–ranged adhesion (Maugis, 1992). It is accepted that short–ranged adhesion is retrieved semi–analytically when the relaxed Maugis parameter $3 < \lambda_0$ (Johnson and Greenwood, 2008). As suggested by Zhu et al. (2021) this might not be the case in the presence of waviness. To assess what is the minimum relaxed Maugis parameter λ_0 that we must use in our simulations to approach short–ranged adhesion, we perform simulations with relaxed Maugis parameters $\lambda_0 = 3.5$, 7 and 14, for the normalized amplitudes $\alpha = 1.46$ and 2.93.

Fig. 3(a) shows the load-area curves for normalized amplitude $\alpha = 1.46$ with relaxed Maugis parameters $\lambda_0 = 3.5$, 7 and 14. The numerical results overlap each other and Guduru's solution, and therefore, adhesion is short–ranged for all relaxed Maugis parameters $3.5 \leq \lambda_0$. When the normalized amplitude $\alpha = 2.93$, however, as shown in Fig. 3(b) for relaxed Maugis parameter $\lambda_0 = 3.5$, the load–area curve deviates. Hence why we conclude that, with increased magnitude of normalized amplitude α, one must consider relaxed Maugis parameters $7 \leq \lambda_0$ to recover short–ranged adhesive, contact mechanics.

To show why a larger Maugis parameter is needed to achieve short–ranged adhesion, Fig. 3(c) gives the pressure profiles that correspond to the relaxed Maugis parameters $\lambda_0 = 3.5$, 7 and 14, for normalized amplitude $\alpha = 2.93$ and normalized wavelength $\beta = 1.87$, at the dimensionless load $\bar{w} = -1.8$. Only half the contact area is shown because of line symmetry about $x = 0$. The oscillations on the normalized pressure profiles (recall that $\bar{p} = p/\sigma_a$), whose magnitudes depend on the amplitude of the waviness, increase with decreased relaxed Maugis parameter λ_0. As a result, when the relaxed Maugis parameter $\lambda_0 = 3.5$, the normal pressures reach the adhesive traction σ_a not only at the edge of the contact but also at the bottom of one of the pressure waves (around $\bar{x} = 3$). This is on the verge of separating the surfaces and clearly distorts the pressure profile. Hence, the assumptions that adhesion is short-ranged and that the contact area is simply connected do no longer hold. For this to occur, the following condition should be met: for a given relaxed Maugis parameter λ_0, the normalized amplitude α must be so large, that the normal pressure oscillations due to waviness are comparable in magnitude with the adhesive traction σ_a. Owing to the interplay between waviness and adhesion, a larger relaxed Maugis parameter is required, than for smooth contact, to approach the JKR–solution. For the relatively small amplitudes used in this work ($\alpha \leq 2.93$), we find that the relaxed Maugis parameter $\lambda_0 = 7$ suffices.

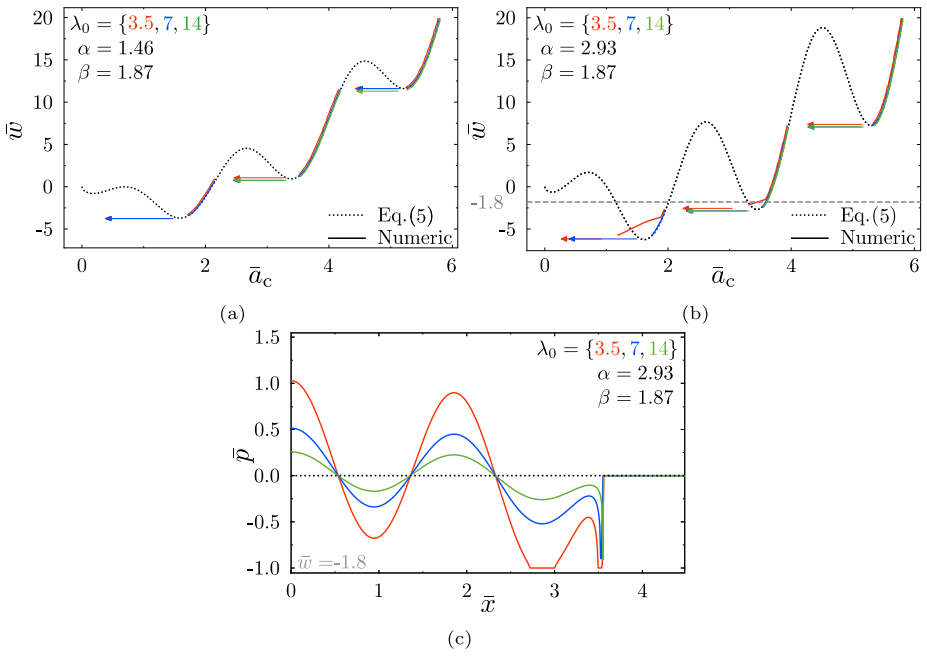

Fig. 3. Load-Area curves during retraction with the normalized wavelength $\beta = 1.87$, relaxed Maugis parameters $\lambda_0 = 3.5$, 7 and 14, for the normalized parameters (a) $\alpha = 1.46$ and (b) 2.93. The dotted lines indicate Guduru's solution (5), the solid lines the numerical solutions, and the arrows unstable jumps. (c) Pressure profiles for normalized amplitude $\alpha = 2.93$ and the load $\bar{w} = -1.8$ as indicated by a light grey dashed line in (b).

5. Wavy viscoelastic contacts

Let us now study the retraction of a wavy, adhesive, infinitely long cylinder from a viscoelastic half–plane. We start by addressing a specific case, with parameters that ensure the contact is simply connected during retraction, namely: normalized amplitude $\alpha = 1.46$; normalized wavelength $\beta = 1.87$; maximum dimensionless load $\bar{w}_{\max} = 20$; retraction rate $\dot{\bar{w}} = \dot{w}\tau / \left(RE_0^* \Delta\gamma_0^2\right)^{1/3} = 1.3{\cdot}10^{-3}$; and, modulus ratio $f_r \equiv E_\infty^*/E_0^* = 10$. The load-area curve during retraction is presented in Fig. 4(a) together with the elastic solution as reference (blue solid line), with the relaxed effective modulus E_0^* (i.e., $\dot{w} \sim 0$); the blue curve indicates an elastic solution, with the relaxed effective modulus E_0^*, while the red line indicates the viscoelastic solution with retraction rate $\dot{\bar{w}} \times 10^4 = 13$. Since the contact area is always simply connected, the elastic solution (blue solid line) follows closely Guduru's analytical solution (5), that is marked with a dark grey dotted line. The viscoelastic curves fall below the dark grey dotted reference, i.e., a larger contact area is found for the same load, which indicates that adhesion is stronger. In the following, we refer to Guduru's solution (5), with the relaxed effective modulus E_0^* as the relaxed limit, because the viscoelastic contact tends to this reference when viscous dissipation becomes negligible.

The increased adhesion provided for by viscous dissipation is traditionally described by an effective work of adhesion $\Delta\gamma_0 \le \Delta\gamma_{\text{eff}} \le f_r \Delta\gamma_0$ (see e.g. Ciavarella and Papangelo, 2021). A straightforward analysis (see e.g. Greenwood and Johnson, 1981) shows that the maximum effective work of adhesion reached due to viscous dissipation is $\Delta\gamma_\infty = f_r \Delta\gamma_0$, that corresponds to an elastic material with the instantaneous effective modulus E_∞^* (Van Dokkum et al., 2021). Guduru's solution for the elastic contact with the instantaneous effective modulus E_∞^*, in the second term on the RHS of Eq. (5a), is indicated by a light grey dotted line in Fig. 4(a), and marks the lower limit to the viscoelastic load–area curves. In the following, we will refer to this solution as the instantaneous limit, given that the viscoelastic contact tends towards it at high retraction rates.

It is important to highlight that the variation in work of adhesion caused by viscoelasticity is a cause of hysteresis during indentation and retraction. While upon retraction adhesion is enhanced, upon indentation adhesion is reduced. Therefore, the load–area curves during retraction reside below the relaxed limit, for indentation they reside above it. Greenwood and Johnson (1981) obtained the limit for the minimum work of adhesion, $\Delta\gamma_0/f_r$, reached upon indentation at high indentation rates. The upper limit to the actual indentation curve is reported in Fig. 4(a) by a magenta dotted line that falls above the relaxed limit (dark grey dotted line). The actual indentation simulation for wavy, viscoelastic cylinders is not presented here, because the decrease in adhesion upon indentation is such that the contact area is no longer simply connected. Evidently, however, the fact that the waviness induces a disconnected contact area upon indentation and a simply connected contact area upon retraction is an additional source of mechanical hysteresis.

As described in Section 4, the elastic solution is characterized by an unstable jump around $\bar{a}_c = 5$ as marked by a yellow circle, where Guduru's analytical solution has a minimum. This jump, however, does not occur in the adhesive, viscoelastic curve. This is in line with what was observed by e.g. Ciavarella and Papangelo (2021) and is rationalized as follows: in an elastic material, the only

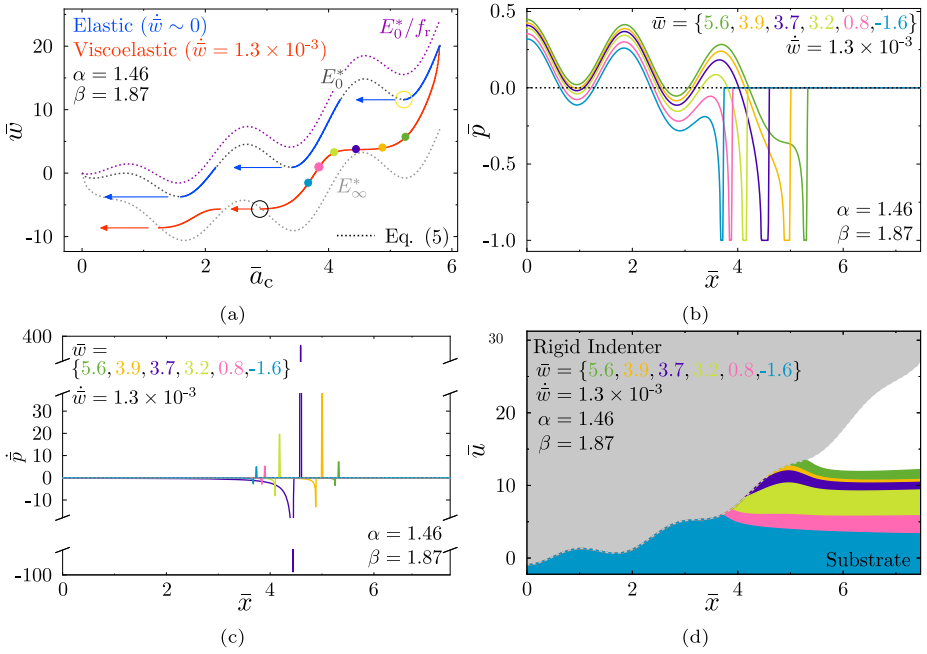

Fig. 4. (a) Load-Area curves during retraction with normalized amplitude $\alpha = 1.46$, normalized wavelength $\beta = 1.87$, relaxed Maugis parameter $\lambda_0 = 7$, maximum normalized load $\bar{w}_{\max} = 20$, retraction rates $\dot{\bar{w}} \sim 0$ and $1.3 \cdot 10^{-3}$, and modulus ratio $f_r = 10$. The dark grey dotted line indicates Guduru's analytical solution (5) with the relaxed effective modulus E_0^*, the light grey dotted line with the instantaneous effective modulus E_∞^* and the magenta dotted line indicates the instantaneous limit during indentation, with effective modulus E_0^*/f_r. The unstable jumps are indicated with coloured arrows. (b) Pressure, (c) pressure rate, and (d) separation profiles for the loads $\bar{w} = 5.6$, 3.9, 3.7, 3.2, 0.8 and -1.6 as indicated by differently coloured, dot-shaped markers in (a).

equilibrium positions are given by the relaxed limit (dark grey line in Fig. 4(a)). For a viscoelastic material, however, an infinite number of such solutions exist as the effective work of adhesion, $\Delta\gamma_{\text{eff}}$, is allowed to vary freely between $\Delta\gamma_0$ and $\Delta\gamma_\infty$. Therefore, the whole load–area region between the relaxed and instantaneous limits (dark and light grey dotted lines in Fig. 4(a)) provides for stable, quasi-static equilibrium positions. As a result, an unstable jump only occurs when the viscoelastic solution meets the instantaneous limit. Above the instantaneous curve and below the elastic curve, this jump is substituted by a line of rapid load–area reduction where significant viscous dissipation occurs. A similar irreversibility is observed upon crack opening in ductile solids (Landis et al., 2000; Gao and Bower, 2004). The location where the jump starts is indicated by a black circle on the light grey dotted line around the contact area $a_c = 3$ in Fig. 4(a).

To better understand what happens upon the retraction of the wavy, adhesive cylinder, the pressure profiles are presented in Fig. 4(b) at the loads $\bar{w} = 5.6$, 3.9, 3.7, 3.2, 0.8 and -1.6, which correspond to the coloured dot–shaped markers in Fig. 4(a). All the pressure profiles look qualitatively similar, with smooth oscillations that match the waviness of the indenter, and a large attractive normal pressure spike at the edge of the contact. It should be noted that, while the normal pressures induced by the waviness is fairly high, its pressure profile is smooth. When the contact area recedes upon retraction, high pressure rates $\dot{\bar{p}}$ are confined to the edges of the contact, as shown in Fig. 4(c), and consistent with the common assumption in the literature, that the viscous dissipation is concentrated at the edges of intimate contact. Of course, this holds true only when the retraction rate does not exceed a given *a priori* unknown threshold such that adhesion is still short-ranged.

It is interesting to observe in Fig. 4(b) that the size of the adhesive region at the edges of the contact is different at different loads. The load $\bar{w} = 3.7$, as indicated by the purple curves in Figs. 4(b)–4(d), has the widest adhesive region of all loads we investigate. This is because the purple profile in Fig. 4(b) corresponds to a point, indicated with a purple dot-shaped marker on the load-area curve in Fig. 4(a), with the smallest slope $\mathrm{d}\bar{w}/\mathrm{d}\bar{a}_c$: a minute reduction in the applied load leads to a large drop in the contact area. Therefore, the velocity of the contact area reduction is the highest at that point, which leads to an increase in normal pressure rate that stiffens the substrate locally, thus holding the surfaces closer together and increasing adhesion. In the relaxed limit, an unstable jump occurs; in the viscoelastic case, instead, the acceleration in contact area reduction induces an increase in the effective work of adhesion $\Delta\gamma_{\text{eff}}$, that allows for a quasi-static stable contact to be attained and the mechanical instability is avoided.

The deformed profile of the substrate and the indenter are presented in Fig. 4(d). Here, we fix the position of the cylinder and let the substrate separate from it, for a clear visualization. Again, the deformed profiles presented coincide with the coloured, dot-shaped markers in Fig. 4(a) corresponding to the loads $\bar{w} = 5.6$, 3.9, 3.7, 3.2, 0.8 and -1.6. Unsurprisingly, the point at which the contact area reduces fastest coincides with the contact edge at a local maximum in the waviness. In Fig. 4(d), it is notable that the angle formed between the profile of the indenter and the substrate changes. Close to the peak in the waviness, this angle is highly acute, since the substrate stiffens as the edge of contact accelerates, and the gap reduces. A final observation in this regard

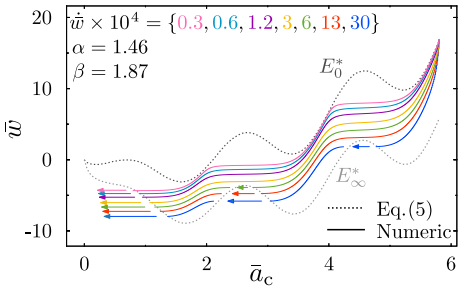

Fig. 5. Load–Area curves during retraction with normalized amplitude $\alpha = 1.46$, normalized wavelength $\beta = 1.87$, relaxed Maugis parameter $\lambda_0 = 7$, maximum load $\bar{w}_{\max} = 20$, and modulus ratio $f_r = 10$, for retraction rates $\dot{\bar{w}} \times 10^4 = 0.3$, 0.6, 1.2, 3, 6, 13 and 30. The dotted, dark and light grey lines indicate the relaxed and instantaneous limit, respectively, the solid lines the numerical solutions, and the coloured arrows the unstable jumps.

is that a JKR–type of adhesion is characterized by an obtuse contact angle, due to short–ranged adhesion (see e.g. the profiles at the loads $\bar{w} = 5.6$ and -1.6 in Fig. 4(d)). Hence, it is apparent from the results presented in Fig. 4(d) that with viscous dissipation and waviness the contact departs from the JKR–limit. This effect can be incorporated in the Maugis parameter by introduction of an effective Maugis parameter $\lambda_{\text{eff}} = \Delta\gamma_{\text{eff}}(R/E_0^{*2}\Delta\gamma_{\text{eff}})^{1/3}/\delta_{\max} \leq \lambda_0$ (Van Dokkum et al., 2021), that decreases when the effective work of adhesion increases due to viscous dissipation.

In the remainder of this section, we study how the adhesive contact response is affected by the retraction rate $\dot{\bar{w}}$; the range of adhesion, characterized by the relaxed Maugis parameter λ_0; the waviness, characterized by the normalized amplitude α and wavelength β; and, the initial indentation, characterized by the maximum load $\bar{w}_{\max}$. As in Fig. 4(a), so in the following, we compare the results with the relaxed and instantaneous limits to facilitate their interpretation.

5.1. Retraction rate

The effect of the retraction rate $\dot{\bar{w}} \times 10^4 = 0.3,\ 0.6,\ 1.2,\ 3,\ 6,\ 13$ and 30 on the load-area curve is presented in Fig. 5. As expected, one observes a monotonic trend; the load-area curve approaches the relaxed limit at small retraction rates and the instantaneous limit at high retraction rates. Towards the relaxed limit, the viscoelastic response closely follows Guduru's analytical solution (5) with the relaxed effective modulus E_0^*. As explained before, however, the unstable jumps are no longer present and, instead, a rapid yet stable decrease in contact area is observed for retraction rates $\dot{\bar{w}} \times 10^{-4} \leq 3$.

At high rates $6 \leq \dot{\bar{w}} \times 10^{-4}$, unstable jumps do reoccur. More precisely, these jumps reappear when the load-area curve meets the instantaneous limit as indicated with the black dotted line in Fig. 5. A stable quasi–static equilibrium at loads below the instantaneous limit implies an effective work of adhesion $\Delta\gamma_\infty < \Delta\gamma_{\text{eff}}$. The instantaneous work of adhesion $\Delta\gamma_\infty$ is the upper limit that can be reached due to the material stiffening caused by viscous dissipation. As discussed in the previous Section 4, no stable contact configurations thus exist for loads below that (instantaneous) limit.

5.2. Range of adhesion

While a smooth elastic contact can be considered to have short–ranged adhesion for a Maugis parameter $3 < \lambda_0$ (Johnson and Greenwood, 2008), we have shown in Section 4 that, if a wavy elastic contact has a significant value of amplitude α, a larger value of relaxed Maugis parameter λ_0 is needed. Hence, it is interesting to study how the contact response changes with increasing Maugis parameter also in the case of viscoelastic wavy contacts. An additional reason why it is important to consider a range of Maugis parameters that depart from the limit, is that in the limit $\lambda_0 \to \infty$, the normal pressure at the edge of the contact reaches an infinite value. Hence, the instantaneous limit is reached with any finite retraction rate, which is contrary to common experimental observations (Greenwood, 2004).

Fig. 6(a) presents the load-area curves for the relaxed Maugis parameters $\lambda_0 = 3.5,\ 7$ and 14. Recall that increasing the Maugis parameter corresponds to increasing the work of adhesion $\Delta\gamma_0$, reducing the interaction range $\delta_{\max}$, or making the system larger and/or stiffer. The Maugis parameter has a similar effect as the retraction rate, i.e., when increased the instantaneous limit is approached as the viscous dissipation at the edges of the contact increases. This similarity arises because viscous dissipation depends on the rate of change in normal traction at the edges of contact. Indeed, an increase in Maugis parameter leads to a sharper and more negative pressure peak at the edge of the contact and hence increases the pressure rate's magnitude there.

Fig. 6(b) presents solutions for normalized amplitude $\alpha = 2.93$. The simulations with relaxed Maugis parameters $\lambda_0 = 7$ and 14 follow the expected behaviour of short–ranged adhesion. However, the simulation with relaxed Maugis parameter $\lambda_0 = 3.5$ does not, as the unstable jumps do not occur when the curve meets the instantaneous limit. It should be noted that aforementioned deviation is stronger for viscoelastic substrates than elastic ones, as viscous dissipation reduces the effective Maugis parameter (Van Dokkum et al., 2021). Hence, both waviness and viscoelasticity contribute towards making adhesive, contact mechanics depart from short–ranged adhesion, and a larger relaxed Maugis parameter $3.5 \leq \lambda_0$ is necessary to ensure that short–ranged, adhesive behaviour is recovered. Herein, relaxed Maugis parameter $7 \leq \lambda_0$ suffice. We though emphasize that this lower limit depends on the chosen normalized waviness parameters α and β, as well as retraction rate $\dot{\bar{w}}$. Also, note that the Maugis parameter we used is the classic one, designed for smooth cylindrical contact and thus includes only the Hertzian radius as geometric parameter.

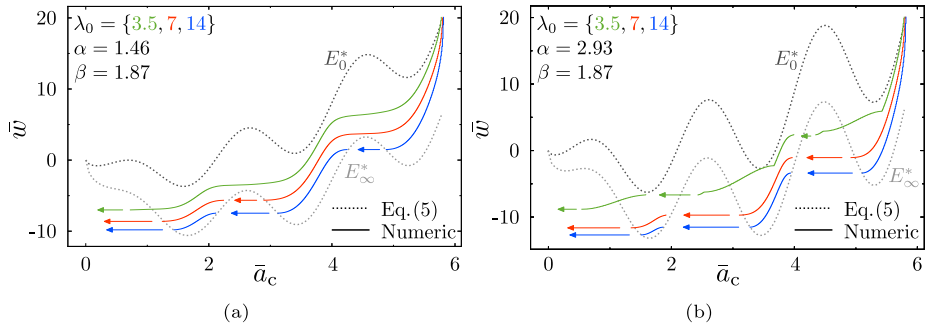

Fig. 6. Load–Area curves during retraction with normalized wavelength $\beta = 1.87$, maximum load $\bar{w}_{max} = 20$, retraction rate $\dot{\bar{w}} \times 10^4 = 6$, modulus ratio $f_r = 10$ and relaxed Maugis parameters $\lambda_0 = 3.5$, 7 and 14, for the normalized amplitudes (a) $\alpha = 1.46$ and (b) 2.93. The dotted, dark and light grey lines indicate the relaxed and instantaneous limit, respectively, the solid lines the numerical solutions, and the coloured arrows the unstable jumps.

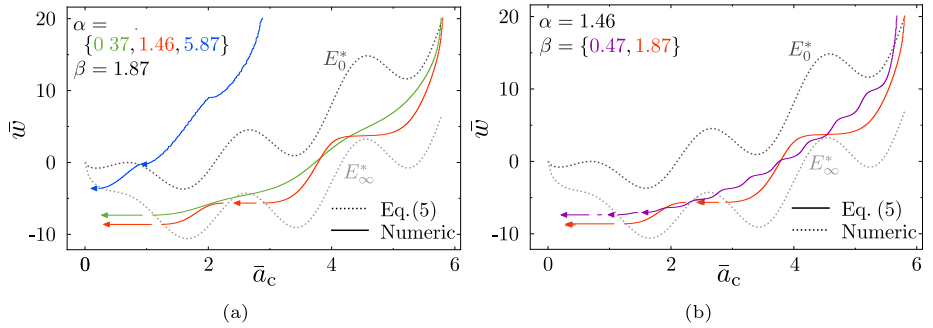

Fig. 7. Load–Area curves for retraction with relaxed Maugis parameter $\lambda_0 = 7$, maximum load $\bar{w}_{max} = 20$, retraction rate $\dot{\bar{w}} \times 10^4 = 13$ and modulus ratio $f_r = 10$, for (a) normalized amplitudes $\alpha = 0.37$, 1.46 and 5.87, and (b) normalized wavelengths $\beta = 0.47$ and 1.87. The dotted, dark and light grey lines indicate the relaxed and instantaneous limit, respectively, with normalized amplitude $\alpha = 1.46$ and normalized wavelength $\beta = 1.87$, and the coloured arrows indicate unstable jumps.

5.3. Waviness

The effect of the normalized amplitude α and normalized wavelength β on the viscoelastic contact response is presented in Fig. 7. For that, we use $\alpha = 0.37$, 1.46, 5.87 and $\beta = 0.47$ and 1.87. The effect of normalized parameters α and β is analogous to that observed for elastic indentation (see Section 4): the normalized amplitude α controls the amplitude of the load–area oscillations; and, the normalized wavelength β the wavelength of these load–area oscillations.

As shown in Section 5.1, the quasi–static solution falls between the relaxed and instantaneous limits (such limits are only included in the figures for one case with visualization purpose). This holds for normalized waviness parameters $\alpha = 1.46$ and $\beta = 1.87$ in Fig. 7 as well. For normalized amplitudes $\alpha = 0.37$ and 1.46 in Fig. 7(a), and for normalized wavelengths $\beta = 0.47$ and 1.87 in Fig. 7(b), the contact area is simply connected during retraction, therefore the two limits are represented by Guduru's curves (5) with the relaxed and instantaneous modulus, E_0^* and E_∞^*, respectively. For normalized parameters $\alpha = 5.87$ and $\beta = 1.87$ in Fig. 7(a), the contact area is not always simply connected, therefore Guduru's solution is not applicable and the limiting behaviours are only found numerically (not shown here).

An important observation on the unstable jumps is that their occurrence enhances with increasing normalized parameter(s) α and/or β. This is because they both have the effect of increasing the amplitude of the oscillations in the load–area curve, and therefore the possibility that one of their minima meets the instantaneous limit. Indeed, it is clear from Fig. 7(b) that, while a pronounced unstable jump occurs for normalized parameters $\alpha = 1.46$ and $\beta = 1.87$, very few mechanical instabilities are present with normalized parameters $\alpha = 1.46$ and $\beta = 0.47$.

5.4. Initial indentation

In order to asses the effect of the initial indentation, i.e., the indentation depth from which retraction starts, we plot in Fig. 8, the load–area curves with normalized amplitudes $\alpha = 1.46$ and 5.87 for the maximum loads $\bar{w}_{max} = 20$, 40 and 80. For normalized amplitude $\alpha = 1.46$ in Fig. 8(a), the load-area curves follow predominantly the same retraction path. Only at the onset of retraction a transition period is observed, that occurs while the contact departs from the relaxed limit ($\dot{\bar{w}} \sim 0$) as retraction initiates, towards a pseudo "*steady–state*", i.e. the contact mechanical response becomes independent of the initial state. Note that the starting point of

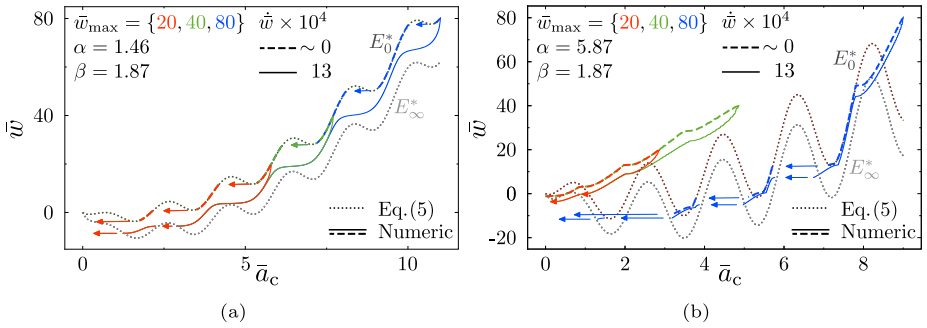

Fig. 8. Load–Area curves during retraction starting from maximum loads $\bar{w}_{\max}$ = 20, 40 and 80. The dimensionless wavelength is β = 1.87, the relaxed Maugis parameter λ_0 = 7, the retraction rate $\dot{\bar{w}} \times 10^{-4}$ = 13 and the modulus ratio f_r = 10, for the normalized amplitudes (a) α = 1.46 and (b) 5.87. The dotted, dark and light grey lines indicate the relaxed and instantaneous limit, respectively, the solid and dashed lines the numerical solutions, and the coloured arrows the unstable jumps.

the viscoelastic curves coincides with the relaxed limit, as the initial indentation is done assuming that the substrate is elastic and is characterized by the relaxed effective elastic modulus E_0^*. The aforementioned behaviour is also observed for smooth cylinders in Van Dokkum et al. (2021).

For normalized amplitude α = 5.6 in Fig. 8(b), the increase in maximum load $\bar{w}_{\max}$ from 40 to 80 leads to a change in the load-area curves during retraction. This difference is due to the change in connectedness of the contact area. For the maximum loads $\bar{w}_{\max}$ = 20 and 40, the contact area is disconnected, while it is simply connected for the maximum load $\bar{w}_{\max}$ = 80. Therefore, the retraction paths differ drastically, as seen in Fig. 8(b), where Guduru's elastic solution (5) is valid, as the contact area becomes simply connected. It is noteworthy that the elastic solution ($\dot{\bar{w}} \sim 0$), as indicated by dashed coloured lines in Fig. 8, shows the same trend though, which confirms that the effect of initial indentation is mostly caused by roughness and negligibly affected by viscoelasticity.

5.5. Viscoelastic parameter

As discussed in Sections 5.1 and 5.2, both an increase in the retraction rate and in the relaxed Maugis parameter lead to a similar effect: the contact response approaches the instantaneous limit. This is in line with what is observed for smooth Hertzian, viscoelastic contact, for instance in Van Dokkum et al. (2021), Müser and Persson (2022), Violano and Afferrante (2022a). In our previous work (Van Dokkum et al., 2021), we propose a new dimensionless parameter that includes both retraction rate and Maugis parameter, and allows to predict the viscoelastic effect, i.e., to establish how far the adhesive contact is from the relaxed or the instantaneous limits. In the context of the retraction of a given smooth Hertzian, that dimensionless parameter is

$$\chi_{ve} \equiv \frac{\dot{w}\tau}{E_0^* \delta_{\max}} \lambda_0 = \frac{\dot{w}\tau\sigma_a^2}{E_0^* \Delta\gamma_0^2} \left(\frac{R\Delta\gamma_0^2}{E_0^{*2}} \right)^{1/3} = \dot{\bar{w}} \lambda_0^2, \tag{6}$$

where the retraction velocity (v_z in Van Dokkum et al., 2021), is here replaced with $\dot{w}/E_0^*$ to directly link the viscoelastic parameter χ_{ve} to the applied retraction rate. For a smooth adhesive contact, characterized by short–ranged adhesion, an increase in viscoelastic parameter χ_{ve} directly correlates with an increase in the viscoelastic dissipation.

The viscoelastic parameter, though introduced for smooth contacts, was applied in Van Dokkum et al. (2021) to experimental works on rough contacts in the literature, and was found to correlate with the amount of viscoelastic losses. Therefore, we herein hypothesize that the effect of waviness can be decoupled from that of viscoelasticity. If this is the case, the viscoelastic parameter should still directly correlate to the amount of viscous dissipation and thus correspond to a unique retraction curve for a given normalized amplitude of the waviness. To test whether this is indeed the case, we perform simulations with constant viscoelastic parameter χ_{ve}, while varying the relaxed Maugis parameter and loading rate, for contacts with various normalized amplitude.

In Fig. 9, the load–area curves are presented for normalized parameters α = 1.46 and 2.93, and β = 1.87, relaxed Maugis parameters λ_0 = 3.5, 7 and 14, and retraction rates $\dot{\bar{w}} \times 10^3$ = 0.16, 0.67 and 2.70, and 0.32, 1.34 and 5.40, which correspond to constant viscoelastic parameters χ_{ve} = 0.033 and 0.066, respectively; the solutions for normalized amplitude α = 1.46 is indicated by solid coloured lines, 2.93 with dashed coloured lines, and 5.87 with dashed–dotted coloured lines. For the smallest normalized amplitude, α = 1.46, the load-area curves for a given viscoelastic parameter χ_{ve} indeed overlap. There is a very small deviation only for the curves with the smallest Maugis parameter. This is evidence that the effect of waviness is uncoupled from that of viscoelasticity, when adhesion is short–ranged (e.g. small amplitude and large relaxed Maugis parameter).

As reported in Section 4, waviness induces a transition from short- to long-range adhesion. Therefore, for the intermediate amplitude, α = 2.93, the curves with largest relaxed Maugis parameters overlap, while the curves for the smallest relaxed Maugis parameter deviate markedly among each other, while the unstable jumps occur at different loads.

For the cases with largest amplitude, α = 5.87, characterized by a non–connected contact area and no instabilities, the curves are close to each other but non–overlapping, while the curves with smallest relaxed Maugis parameter are characterized by the largest

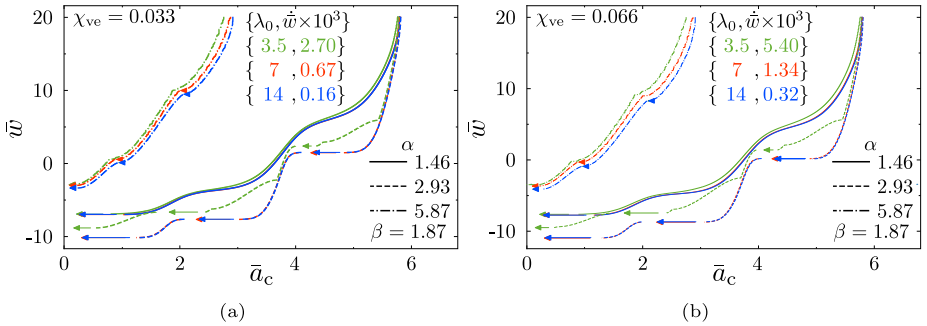

Fig. 9. Load–Area curves during retraction with normalized amplitudes α = 1.46, 2.93 and 5.87, normalized wavelength β = 1.87, maximum load $\bar{w}_{max}$ = 20, modulus ratio f_r = 10 and relaxed Maugis parameters λ_0 = 3.5, 7 and 14, for retraction rates (a) $\dot{\bar{w}} \times 10^3$ = 0.16, 0.67 and 2.70, and (b) 0.32, 1.34 and 5.40, that result in constant dimensionless parameters (a) χ_{ve} = 0.033 and (b) 0.066, respectively.

viscous losses. Also in this case, we believe that the difference between the three curves is due to a departure from short–ranged adhesion that is already present for the intermediate relaxed Maugis parameter, given that the amplitude is larger. This is confirmed by the facts that the difference increases as the relaxed Maugis parameter λ_0 reduces and that the difference between the three curves for the largest dimensionless amplitude is larger when the viscoelastic parameter χ_{ve} increases. We conclude that the viscoelastic parameter χ_{ve} retains its predictive power in the presence of waviness, as long as adhesion remains short–ranged. This proves that, in the limit of short-ranged adhesion, the effect of waviness and viscoelasticity are independent. The viscoelastic parameter helps us identify the limits of this independence: as waviness becomes larger, while the remaining parameters are constant, adhesion becomes more long-ranged and hence affects the location and magnitude of viscous dissipation. Of course, the waviness at which this occurs depends on the relaxed Maugis parameter λ_0.

5.6. Pull–off

Finally, we look at the pull–off load, that is the maximum tensile load reachable upon retraction, just before the indenter snaps out of contact. For a smooth cylindrical indenter separating from an elastic substrate, JKR theory (Johnson and Greenwood, 2008) indicates that this load is

$$\bar{w}_{PO}^{JKR} = -(3/4)(4\pi E_0^* R \Delta\gamma_0^2)^{1/3}, \tag{7}$$

that is negative (tension) when adhesion allows for the indenter to pull on the substrate. A common way to assess how much viscoelasticity and waviness enhance hysteresis is to look at how the pull–off load increases (Ciavarella and Papangelo, 2021). This is best shown by scaling the numerically obtained pull-off load $\bar{w}_{PO}$ with the theoretical pull–off load $\bar{w}_{PO}^{JKR}$.

In Fig. 10, we show the pull-off load $\bar{w}_{PO}$ as a function of the retraction rate $\dot{\bar{w}}$, for normalized amplitudes α = 0, 0.37, 1.46 and 2.93, and normalized wavelengths β = 0.47, 0.93 and 1.87; the pull–off loads are indicated with plus–shaped coloured markers. The relaxed limit is given in Fig. 10(a) with plus–shaped coloured markers as a reference and indicated by "El" as well. By extrapolating the solid lines, which connect the data point to help visualizing the trends, one sees that this relaxed limit is only approached at very low retraction rates.

We consider first a smooth indenter (blue curve, with normalized amplitude α = 0 in Fig. 10(a)) and reproduce the JKR results: a value of one is obtained in the relaxed limit. In the instantaneous limit, definition (7) holds, provided that the work of adhesion is replaced by the instantaneous work of adhesion $\Delta\gamma_\infty$. Since the modulus ratio $\Delta\gamma_\infty/\Delta\gamma_0 = f_r = 10$, the pull-off load in the instantaneous limit approaches $\bar{w}_{PO,\infty}/\bar{w}_{PO}^{JKR} \sim f_r^{2/3} \approx 4.6$. Indeed, the load–rate curve shows that the pull–off load asymptotically tends to the expected value. Consistent with the literature, we find that the pull–off load vs. retraction rate curve is straight at intermediate rates (Ciavarella and Papangelo, 2021), showing that the effective work of adhesion is a power function of the retraction rate.

Turning now to the effect of waviness, we see that the ratio $\bar{w}_{PO}/\bar{w}_{PO}^{JKR}$ increases even in the relaxed limit, consistent with the elastic results provided by Guduru (2007), who shows that small roughness enhances adhesion. An increase in normalized wavelength α increases the amplitude of the load-area oscillations and hence allows larger pull–off loads to be reached. An increase in normalized parameter β has a more moderate effect, although an increase in the pull–off load with the roughness wavelength is still observed in Fig. 10(b). The reason is seen in Fig. 2(b): while the amplitude of the load-area oscillations created by the waviness is the same, the oscillations' minima occur at lower loads. We must give, however, a cautionary notice in that this trend only holds for small values of normalized amplitude α and mi–ranged values of normalized wavelength β. As discussed in Section 4, the effect of waviness vanishes at both large and small values of normalized wavelength β because a smooth indenter is recovered. Similarly, the pull–off load's increase due to waviness will also disappear at high values of normalized amplitude α, due to the loss of connectedness in the contact area (Zhu et al., 2021).

When viscoelasticity is considered, a further increase in the pull–off load is observed. For all values of normalized amplitude α and normalized wavelength β, the load–rate curves simply shift to higher loads. This indicates that the effect of viscoelasticity is

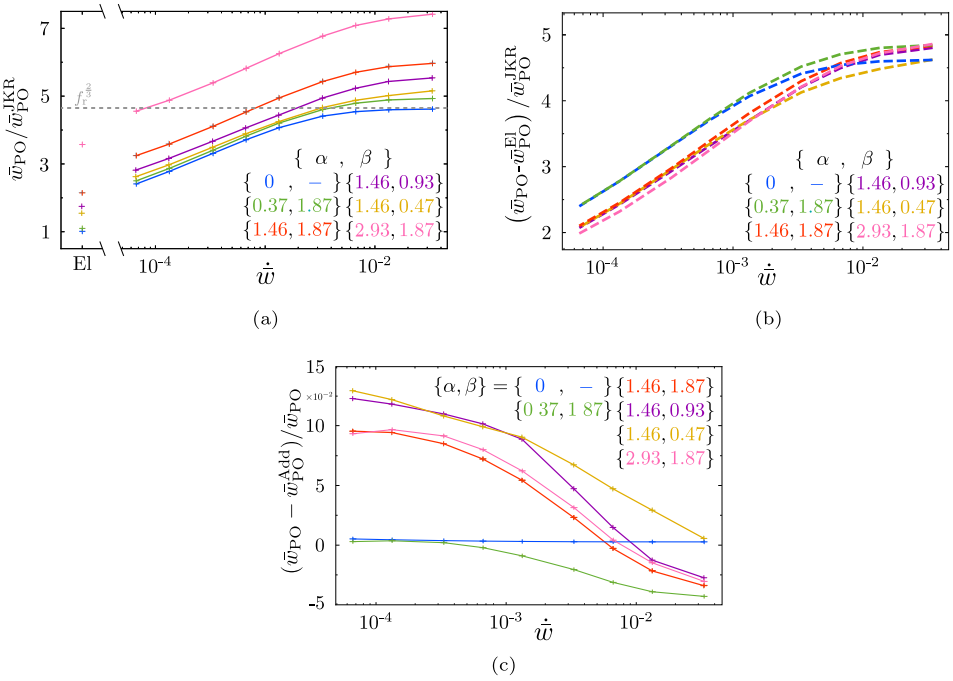

Fig. 10. (a) The scaled pull-off load $\bar{w}_{\mathrm{PO}}/\bar{w}_{\mathrm{PO,JKR}}$, (b) the scaled, shifted pull-off load $\left(\bar{w}_{\mathrm{PO}}-\bar{w}_{\mathrm{PO}}^{\mathrm{El}}\right)/\bar{w}_{\mathrm{PO}}^{\mathrm{JKR}}$ and (c) the scaled error $\left(\bar{w}_{\mathrm{PO}}-\bar{w}_{\mathrm{PO}}^{\mathrm{Add}}\right)/\bar{w}_{\mathrm{PO}}$ as functions of the retraction rate $\dot{\bar{w}}$ for normalized parameters $\{\alpha,\beta\}=\{$ 0,-$\}$, $\{0.37,1.87\}$, $\{1.46,1.87\}$, $\{1.16,0.93\}$, $\{1.46,0.47\}$ and $\{2.93,1.87\}$. The relaxed limit ($\dot{\bar{w}}\sim 0$) in (a) is indicated by plus-shaped coloured markers as well.

predominantly independent of waviness, as shown in Section 5.5, and that both dissipative contributions add to reach the observed pull–off load. To prove this point, we plot in Fig. 10(b) the scaled, shifted pull–off load, i.e., the pull–off load in the relaxed limit $\bar{w}_{\mathrm{PO}}^{\mathrm{El}}$ is subtracted from the observed pull–off load $\bar{w}_{\mathrm{PO}}$. The difference between the observed pull–off load and the additive estimate $\bar{w}_{\mathrm{PO}}^{\mathrm{Add}}(\alpha,\beta)\equiv\bar{w}_{\mathrm{PO}}(\alpha=0)+\bar{w}_{\mathrm{PO}}^{\mathrm{El}}(\alpha,\beta)$ is given in Fig. 10(c). For the various values of the normalized amplitude α, the additive estimation is very close to the numerically computed one and the difference is always smaller than 10%. This error is found to be larger for the range of normalized wavelength β we selected, but it still remain fairly low, below 13%.

This shows that, as previously hypothesized, the effects of waviness and viscoelasticity are nearly independent and additive, in short–ranged adhesive contact, at least for the range of parameters studied in this paper. This entails that one should be able to estimate the viscoelastic losses of a rough adhesive surface by knowing the elastic response of the adhesive rough surface and the viscoelastic response of the corresponding smooth contact.

6. Discussion

The results presented in this work show that both waviness and viscoelasticity increase the effective work of adhesion during retraction and hence adhesive hysteresis. The two contributions are found to be near independent, as discussed in the following.

Upon retraction of the indenter, the viscoelastic load–area curves for smooth contacts follow a path parallel to the JKR solution, characterized by an increased effective work of adhesion (Van Dokkum et al., 2021; Violano et al., 2021a). The load–area curves for wavy contact are also shifted to lower loads with respect to the reference solution by Guduru (2007) (see Section 5 and Ciavarella and Papangelo, 2021). In this case, however, the distance between the viscoelastic and elastic curves is not constant as in elastic rough contacts, because the effective work of adhesion oscillates with the retraction velocity. Both elastic and viscoelastic rough contacts are characterized by adhesive hysteresis, but their origins differ. In an elastic, wavy contact, it is the dissipation of energy in the unstable jumps that causes adhesive hysteresis (Guduru and Bull, 2007), as the elastic jumps upon retraction occur at lower load than upon indentation. With viscoelasticity, instead, the unstable jumps are replaced by fast quasi-static reduction of the contact area, in which energy is lost due to viscous dissipation. The jump is avoided and the curve instead shifts to lower loads with an increase in the effective work of adhesion. This behaviour is in line with the speculation by Papangelo and Ciavarella (2021a), and Ciavarella and Papangelo (2021) that viscoelasticity "effectively dampens" the elastic instabilities. Of course, energy dissipation upon retraction is larger when viscoelasticity is present, as it occurs throughout the whole retraction process (the load–area curve departs towards lower loads) and not only during localized instabilities. Indeed, the load–area response for viscoelastic substrates alternate between periods of rapid area reduction, which correspond to the "damped" instabilities; and, periods in which the contact area reduces slower, but still more rapidly than elastically.

In our results, we see that unstable jumps are not all damped in viscoelastic contacts, they occur under certain conditions: when the retraction rate (see Sections 5 and 5.1), the surface waviness (see Section 5.3) or the range of adhesion (see Section 5.2) are large. Under one or several of these conditions the quasi-static solution meets the curve that represents the instantaneous limit. Since the effective work of adhesion is bounded, the instability cannot be dampened. These jumps are not observed in Papangelo and Ciavarella (2021a), and Ciavarella and Papangelo (2021) since their theory does not include the instantaneous limit.

Our results demonstrate that, in general, two mechanisms of interfacial toughening are present: viscous and roughness–induced dissipation. The latter can be either in the form of a mechanical instability at high retraction rates or in the form of a fast quasi–static reduction of the contact area, at lower retraction rates when the instability is dampened. Whether the contact area reduction is very fast or occurs through an unstable elastic jump, the result in terms of energy loss is similar. This similarity between the unstable mechanical jump and the damped instability is likely the reason why we find that viscoelasticity and roughness independently contribute to adhesive hysteresis. It is however debatable under which circumstances the instantaneous limit is met in practice. Certainly, as we saw that the stiffening of the material leads to a departure from short–ranged adhesion, the theories that are based on short–ranged adhesion are not always appropriate in that limit.

It is also noteworthy that the modulus ratio $f_r = 10$ we use is small compared to that of most rubbery materials. For instance, $f_r \lessapprox 1000$ in Lorenz et al. (2013). We selected modulus ratio $f_r = 10$ to make the simulations numerically tractable. Larger values of $10 \ll f_r$ would shift the instantaneous limit to more negative loads, and meeting that limit with a short wave amplitude would require a much larger retraction rate or relaxed Maugis parameter. It is also true, that an increase in roughness amplitude, which is reasonable in a real roughness, increases the amplitude of the load–area oscillations. This makes it more likely for the viscoelastic load–area curve to meet the instantaneous limit. It remains up to future investigations to study the combination of realistic roughness and modulus ratios.

Kesari and collaborators (Kesari et al., 2010; Deng and Kesari, 2019) find that hysteresis depends on the maximum load reached before retraction. In our results, the only dependence is attributable to a change in connectedness in the contact area. In our results, instead of a continuous variation with load, we find a sharp transition: at low maximum indentation $\bar{w}_{\max}$, a given path is followed, owing to the non-connectedness of the contact; above a certain load, the contact abruptly becomes simply connected and a completely different path is followed. A more continuous dependence of the retraction path with the maximum indentation load is seen in Kesari et al. (2010), and Deng and Kesari (2019). An important difference between the work by Kesari et al. (2010) and ours is that he considers multi–asperity rough contacts, while ours considers a single wavelength roughness. This is why in our simulations the change in connectivity is abrupt and depends on a single length scale, while in realistic rough contacts several length scales induce small changes in the connectedness of the contact area (Carbone et al., 2015). It is thus reasonable to expect that in a simulation that considers realistic roughness, the dependence on maximum load is continuous, and therefore more in agreement with experimental observations (Kesari et al., 2010; Deng and Kesari, 2019). It is anyhow noteworthy that in our simulations the dependence on initial contact is unaltered by viscoelasticity.

A comment is made in regard to when adhesion is short–ranged. As shown in Fig. 6, a value of the relaxed Maugis parameter λ_0 much larger than three is necessary to ensure that adhesion of a wavy viscoelastic contact can be considered short-ranged. The combined effect of viscoelasticity and waviness is responsible for this (see Sections 5.2 and 5.3). Viscoelasticity is known to toughen the contact and thus decrease the effective Maugis parameter (Van Dokkum et al., 2021; Ciavarella and Papangelo, 2021) and waviness is found to have a similar effect by increasing the work of adhesion. While we find that the relaxed Maugis parameter $7 \leq \lambda_0$ suffices for the contact to display short–ranged adhesion, higher relaxed Maugis parameters are expected to be necessary when the waviness is more prominent or viscoelasticity effects are stronger. For instance, for a viscoelastic material with modulus ratio $f_r = 1000$, $\lambda_0 \approx 1000$ is needed to retain short–ranged adhesion in the instantaneous limit (Ciavarella, 2021b), while $\lambda_0 \approx 100$ was required for $f_r = 100$. This is probably not an issue in macroscopic soft contacts, where the Maugis parameter λ_0 is very large (Baney and Hui (1997) estimate $\lambda_0 = 2.2 \cdot 10^4$). However, the magnitude of the effective Maugis parameter becomes important in mirco– and nano–mechanics (Neupane et al., 2021; Jiang et al., 2021; Das and Chasiotis, 2021), where the relaxed Maugis parameter decreases with the length scale. While even at those length-scales, adhesion is still short–ranged, a combination of surface roughness and viscoelasticity can make adhesive contact mechanics depart from short– towards long–ranged adhesion.

We make a final point regarding the relative influence of waviness and viscoelasticity. In our results, both contributions have a similar influence on hysteresis, while Ciavarella and Papangelo (2021) observe that viscoelasticity dominates over roughness. The apparent discrepancy is just caused by our choice of a small viscoelastic modulus. We have shown that the contribution to the pull–off load of waviness and viscoelasticity is additive, and therefore it is to be expected that for larger values of the modulus ratio E^*_∞/E^*_0 also in our simulations viscoelasticity would dominate.

7. Conclusions

In this work, we consider the two most cited sources of hysteresis in soft adhesive contacts: viscoelasticity, and surface roughness. The former is considered using the Zener model, and the latter is simplified to a single wave, superimposed on the profile of a rigid, cylindrical indenter. By studying the load–area curves during retraction of the indenter, we corroborate that viscoelasticity "effectively dampens" the mechanical instabilities caused by waviness, as long as the instantaneous limit is not reached. When the instantaneous limit is met, which typically happens before jump–out of contact, mechanical instabilities reappear. The occurrence of these instabilities is enhanced by increased amplitude and a decreased range of adhesive interaction, and a simply connected initial contact area. Even when the mechanical instability is dampened by viscoelasticity, the effect is still a fast reduction of the contact area at near constant load, thus similar to that of an instability. The viscoelastic, wavy contact load–area response is thus

characterized by a "slow" viscoelastic peeling interspersed with fast decreases in contact area at near constant loads. Therefore the effects of waviness and viscoelasticity on adhesive hysteresis are approximately uncoupled, in the regime where the viscoelastic effects are confined to the edges of the contacts. This is confirmed by the fact that our viscoelastic parameter, which uniquely characterizes the amount of viscous losses in an adhesive smooth contact, is single valued also when waviness is present.

Both waviness and viscoelasticity contribute to stiffening of the adhesive contact, and thus to a departure from short–ranged towards long–ranged adhesion. This is relevant because many theoretical and numerical predictions of adhesive contact behaviour rely heavily on the short-ranged adhesion assumption. More importantly, the contribution of waviness and viscoelasticity to adhesive hysteresis is found to be near additive: the pull–off load at a given retraction rate is approximately given by the sum of the pull-off load due to viscoelasticity in a smooth contact and that of a wavy, elastic contact. In this study, both waviness and viscoelasticity contribute significantly to hysteresis. This is because we considered a ratio between instantaneous and relaxed moduli of magnitude of ten; for larger values of this ratio and the same waviness, the effect of viscoelasticity would dominate.

The dependence of the pull–off load on the initial load is found to be uncorrelated to viscoelasticity. Presumably, the effect of initial indentation observed experimentally is to be attributed to changes in connectedness of the contact area at different loads, but this must be further investigated with studies that include realistic roughness.

Our results are limited by the simplicity of the descriptions of viscoelasticity, adhesive interaction and surface roughness. Additional work is required to establish whether our conclusions extend to realistic rough contacts.

CRediT authorship contribution statement

Francesc Pérez-Ràfols: Conceptualization, Software, Data analysis, Data curation, Investigation, Writing – original draft. **Jan Steven Van Dokkum:** Conceptualization, Software, Data analysis, Data curation, Investigation, Writing & Editing. **Lucia Nicola:** Conceptualization, Supervision, Writing – review & editing, Funding acquisition.

Declaration of competing interest

The authors declare that they have no known competing financial interests or personal relationships that could have appeared to influence the work reported in this paper.

Data availability

Data will be made available on request.

Acknowledgements

LN acknowledges funding from the European Research Council (ERC) under the European Union's Horizon 2020 research and innovation programme (grant agreement no. 681813).

Appendix A. Viscoelastic GFMD pseudo-code

1. Setup rigid indenter with initial surface topography $h(x)_{t_n=0}$;
2. Determine a damping coefficient such that all modes are critically and/or under-damped, and calculate the dimensionless equilibrium time t^*_{equil} for a given dimensionless time-step Δt^*;
3. Loop over iteration n with time–step Δt till the period t_{final} is reached. Give the location of the rigid indenter as $z(x)^{\text{indenter}}_{t_n+\Delta t} = h(x-\delta^x_{t_n+\Delta t})_{t_n=0}+\delta^z_{t_n+\Delta t}$, where $\delta^z_{t_n+\Delta t}$ and $\delta^x_{t_n+\Delta t}$ are the normal and tangential displacement of the rigid indenter at time $t_n+\Delta t$, respectively.

(a) Loop over Δt^* till the equilibrium time t^*_{equil} is reached:

- Discrete fast Fourier transform (DFFT) surface displacement $u(x)^{\text{new}}_{t_n+\Delta t}$ using the FFTW3 library (Frigo and Johnson, 2005);
- Calculate viscoelastic restoring load, $\tilde{F}(q)^{\text{visco-elas}}_{t_n+\Delta t} \leftarrow \text{Func.}\{\tilde{u}(q)^{\text{new}}_{t_n+\Delta t}, \tilde{u}(q)_{t_n}, \tilde{F}(q)_{t_n}, \Delta t\}$;
- Add external load and interfacial load, $\tilde{F}(q)^{\text{total}}_{t_n+\Delta t} \leftarrow \tilde{F}(q)^{\text{visco-elas}}_{t_n+\Delta t} + \tilde{F}(q)^{\text{ext}}_{t_n+\Delta t} + \tilde{F}(q)^{\text{if}}_{t_n+\Delta t}$;
- Add damping loads, $\tilde{F}(q)^{\text{total}}_{t_n+\Delta t} \leftarrow -c_{\text{cr}}(q)\left(\tilde{u}(q)^{\text{now}}_{t_n+\Delta t} - \tilde{u}^{\text{old}}(q)_{t_n+\Delta t}\right)/\Delta t^*$, with the critical damping coefficient c_{cr};
- Use the (Störmer)-Verlet algorithm (Störmer, 1912) to solve the equation of motion, $\tilde{u}(q)^{\text{new}}_{t_n+\Delta t} = 2\tilde{u}(q)^{\text{now}}_{t_n+\Delta t} - \tilde{u}(q)^{\text{old}}_{t_n+\Delta t} + \tilde{F}(q)^{\text{d}}_{t_n+\Delta t}(\Delta t^*)^2$;
- Assign $\tilde{u}(q)^{\text{old}}_{t_n+\Delta t} \leftarrow \tilde{u}(q)^{\text{now}}_{t_n+\Delta t}$ & $\tilde{u}(q)^{\text{now}}_{t_n+\Delta t} \leftarrow \tilde{u}(q)^{\text{new}}_{t_n+\Delta t}$;
- Reverse DFFT displacement $u(x)^{\text{new}}_{t_n+\Delta t}$ into real space, and scale displacement $u(x)^{\text{new}}_{t_n+\Delta t}$ with $1/\mathcal{L}$;
- Implement the hard-wall boundary condition, $u(x)^{\text{new}}_{t_n+\Delta t} \leftarrow \min\{u(x)^{\text{new}}_{t_n+\Delta t}, z(x)^{\text{indenter}}_{t_n+\Delta t}\}$;
- Calculate interfacial load with a first order discretization of the gap $F(x)^{\text{if}}_{t_n+\Delta t} \leftarrow \text{Func.}\{u(x)^{\text{new}}_{t_n+\Delta t}, z(x)^{\text{indenter}}_{t_n+\Delta t}\}$ and DFFT to $\tilde{F}(q)^{\text{if}}_{t_n+\Delta t}$.

(b) DFFT displacement $u(x)^{\text{new}}_{t_n+\Delta t}$;

(c) Assign $\tilde{u}(q)_{t_n} \leftarrow \tilde{u}(q)^{\text{new}}_{t_n+\Delta t}$ & $\tilde{F}(q)_{t_n} \leftarrow \tilde{F}(q)^{\text{total}}_{t_n+\Delta t}$.

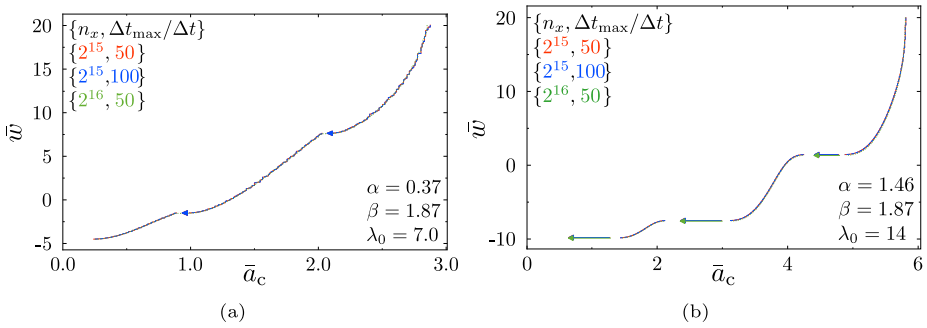

Fig. B.11. Load–Area curves during retraction with normalized wavelength $\beta = 1.87$, maximum load $\bar{w}_{\max} = 20$, retraction rate $\dot{\bar{w}} \times 10^3 = 3$, modulus ratio $f_r = 10$ and the relaxed Maugis parameters and normalized amplitudes, (a) $\lambda_0 = 7$ and $\alpha = 0.37$, and (b) $\lambda_0 = 14$ and $\alpha = 1.46$, respectively. The spatial discretizations and the constant, dimensional time–steps $\{n_x, \Delta t_{\max}/\Delta t\} = \{2^{15}, 50\}$, $\{2^{15}, 100\}$ and $\{2^{16}, 50\}$.

Appendix B. Spatial and temporal convergence

Throughout this work, we use the spatial discretization $n_x = 2^{15}$ and the constant, dimensional time-step $\Delta t = \Delta t_{\max}/50$, where $\Delta t_{\max} = \tau(E^*_\infty - E^*_0)/E^*_\infty$ is the maximum time-step for which a Verlet algorithm is expected to converge (Van Dokkum and Nicola, 2019). In Fig. B.11(a), we show that these values indeed suffice. The numerical, reference solution is characterized by spatial $n_x = 2^{15}$ and temporal discretization $\Delta t_{\max}/\Delta t = 50$. We increase the spatial $n_x = 2^{16}$ and temporal discretization $\Delta t_{\max}/\Delta t = 100$ independently and in accordance with the legends in Fig. B.11.

In Fig. B.11(a), we use the normalized parameters $\alpha = 0.37$ and $\beta = 1.87$, that lead to the highest roughness gradient, and hence is the most demanding in terms of spatial discretization; we also use a retraction rate $\dot{\bar{w}} \times 10^3 = 3$, that is the highest retraction rate in this work, and hence the most demanding in terms of temporal discretization. Higher values of relaxed Maugis parameter for a given work of adhesion require finer spatial discretization, since the adhesive traction increases and the adhesive region narrows. So we present convergence with the solution for the relaxed Maugis parameter $\lambda_0 = 14$, and normalized parameters $\alpha = 1.46$ and $\beta = 1.87$ in Fig. B.11(b). The results indicate that the choices of spatial and temporal discretization suffice for the range of input parameters we consider in this work.

Appendix C. Normalization

The equations governing the contact problem are given by Eqs. (1)–(4). We define the following dimensionless variables

$$\bar{x} = \frac{x}{x_r}, \quad \bar{p} = \frac{p}{p_r}, \quad \bar{t} = \frac{t}{t_r}, \quad \bar{u} = \frac{u}{h_r}, \quad \bar{g} = \frac{g}{h_r}, \quad \bar{w} = \frac{w}{w_r}, \quad \bar{a}_c = \frac{a_c}{x_r} \quad \text{and} \quad \bar{q} = q x_r, \tag{C.1}$$

with the scaling parameters defined as

$$x_r = \left(\frac{R^2 \Delta\gamma_0}{E^*_0}\right)^{1/3}, \quad p_r = \frac{\Delta\gamma_0}{\Delta_{\max}}, \quad t_r = \tau, \quad h_r = \frac{x_r^2}{R} \quad \text{and} \quad w_r = \left(R E^*_0 \Delta\gamma_0^2\right)^{1/3}. \tag{C.2}$$

The governing equations of load–controlled retraction are:

$$\tilde{p}\left(\bar{q},\bar{t}\right) + \dot{\tilde{p}}\left(\bar{q},\bar{t}\right) = -8|\bar{q}|\frac{1}{\lambda_0}\left(\tilde{u}\left(\bar{q},\bar{t}\right) + f_r \dot{\tilde{u}}\left(\bar{q},\bar{t}\right)\right); \tag{C.3a}$$

$$\bar{g}\left(\bar{x},\bar{t}\right) = \frac{\bar{x}^2}{2} + \frac{\alpha}{\pi\beta}\cos\left(\frac{2\pi\bar{x}}{\beta}\right) - \bar{h}_0\left(\bar{t}\right) - \bar{u}\left(\bar{x},\bar{t}\right); \tag{C.3b}$$

with

$$\bar{g}\left(\bar{x},\bar{t}\right) = 0, \qquad \bar{p}(\bar{x},\bar{t}) < 1;$$

$$0 < \bar{g}\left(\bar{x},\bar{t}\right) \le \frac{1}{\lambda_0}, \qquad \bar{p}(\bar{x},\bar{t}) = 1;$$

$$\bar{g}\left(\bar{x},\bar{t}\right) > \frac{1}{\lambda_0}, \qquad \bar{p}(\bar{x},\bar{t}) = 0;$$

and

$$\bar{w}\left(\bar{t}\right) = \bar{w}_{\max} - \dot{\bar{w}}\bar{t} = \lambda_0 \int_{-\bar{\mathcal{L}}/2}^{\bar{\mathcal{L}}/2} \bar{p}\left(\bar{x},\bar{t}\right) \mathrm{d}\bar{x}, \tag{C.3c}$$

where $\bar{\mathcal{L}} = \mathcal{L}/x_r$ is the scaled periodic width. Hence, together with indentation, that is specified by the maximum load ratio $\bar{w}_{\max} = w_{\max}/w_r$, the retraction rate $\dot{\bar{w}} = \dot{w}\tau/w_r$, the surface roughness parameters α and β, the relaxed Maugis parameter λ_0

and the modulus ratio

$$f_r = \frac{E^*_\infty}{E^*_0}, \tag{C.4}$$

control the contact mechanics. In Eq. (C.3), one also finds the scaled indentation $\bar{h}_0 = h_0/x_r$, that indicates the rigid body movement and is directly controlled by load.

References

Afferrante, L., Violano, G., 2022. On the effective surface energy in viscoelastic Hertzian contacts. J. Mech. Phys. Solids 158, 104669. http://dx.doi.org/10.1016/j.jmps.2021.104669.

Baek, D., Hemthavy, P., Saito, S., Takahashi, K., 2017. Evaluation of energy dissipation involving adhesion hysteresis in spherical contact between a glass lens and a PDMS block. Appl. Adhesion Sci. 5 (4), 1–11. http://dx.doi.org/10.1186/s40563-017-0082-z.

Baney, J.M., Hui, C.Y., 1997. A cohesive zone model for the adhesion of cylinders. J. Adhes. Sci. Technol. 11 (3), 393–406. http://dx.doi.org/10.1163/156856197X00778.

Briggs, G., Briscoe, B., 1977. The effect of surface topography on the adhesion of elastic solids. J. Phys. D: Appl. Phys. 10 (18), 2453. http://dx.doi.org/10.1088/0022-3727/10/18/010.

Carbone, G., Pierro, E., Recchia, G., 2015. Loading-unloading hysteresis loop of randomly rough adhesive contacts. Phys. Rev. E 92 (6), 1–8. http://dx.doi.org/10.1103/PhysRevE.92.062404.

Chaudhury, M.K., Weaver, T., Hui, C.Y., Kramer, E.J., 1996. Adhesive contact of cylindrical lens and a flat sheet. J. Appl. Phys. 80 (1), 30–37. http://dx.doi.org/10.1063/1.362819.

Chen, Y.L., Helm, C.A., Israelachvili, J.N., 1991. Molecular mechanisms associated with adhesion and contact angle hysteresis of monolayer surfaces. J. Phys. Chem. 95 (26), 10736–10747. http://dx.doi.org/10.1021/j100179a041.

Chizhik, P., Friedrichs, M., Dietzel, D., Schirmeisen, A., 2020. Tribological analysis of contacts between glass and tungsten carbide near the glass transition temperature. Tribol. Lett. 68 (4), 1–10. http://dx.doi.org/10.1007/s11249-020-01363-0.

Ciavarella, M., 2021a. Improved Muller approximate solution of the pull-off of a sphere from a viscoelastic substrate. J. Adhes. Sci. Technol. 35 (20), 2175–2183. http://dx.doi.org/10.1080/01694243.2021.1882766.

Ciavarella, M., 2021b. An upper bound for viscoelastic pull-off of a sphere with a Maugis-Dugdale model. J. Adhesion 1–14. http://dx.doi.org/10.1080/00218464.2021.1954914.

Ciavarella, M., Greenwood, J., Barber, J., 2017. Effect of tabor parameter on hysteresis losses during adhesive contact. J. Mech. Phys. Solids 98, 236–244. http://dx.doi.org/10.1016/j.jmps.2016.10.005.

Ciavarella, M., Joe, J., Papangelo, A., Barber, J., 2019. The role of adhesion in contact mechanics. J. R. Soc. Interface 16 (151), 20180738. http://dx.doi.org/10.1098/rsif.2018.0738.

Ciavarella, M., Papangelo, A., 2021. On the interaction of viscoelasticity and waviness in enhancing the pull-off force in sphere/flat contacts. Tribol. Lett. 69 (4), 1–11. http://dx.doi.org/10.1007/s11249-021-01488-w.

Coulson, R., Stabile, C.J., Turner, K.T., Majidi, C., 2022. Versatile soft robot gripper enabled by stiffness and adhesion tuning via thermoplastic composite. Soft Robot. 9 (2), 189–200. http://dx.doi.org/10.1089/soro.2020.0088.

Dalvi, S., Gujrati, A., Khanal, S.R., Pastewka, L., Dhinojwala, A., Jacobs, T.D., 2019. Linking energy loss in soft adhesion to surface roughness. Proc. Natl. Acad. Sci. USA 116 (51), 25484–25490. http://dx.doi.org/10.1073/pnas.1913126116.

Das, D., Chasiotis, I., 2021. Rate dependent adhesion of nanoscale polymer contacts. J. Mech. Phys. Solids 156 (May), 104597. http://dx.doi.org/10.1016/j.jmps.2021.104597.

Deng, W., Kesari, H., 2019. Depth-dependent hysteresis in adhesive elastic contacts at large surface roughness. Sci. Rep. 9 (1), 1–12. http://dx.doi.org/10.1038/s41598-018-38212-z.

Dorogin, L., Tiwari, A., Rotella, C., Mangiagalli, P., Persson, B.N.J., 2017. Role of preload in adhesion of rough surfaces. Phys. Rev. Lett. 118 (23), 1–6. http://dx.doi.org/10.1103/PhysRevLett.118.238001.

Dugdale, D.S., 1960. Yielding of steel sheets containing slits. J. Mech. Phys. Solids 8 (2), 100–104. http://dx.doi.org/10.1016/0022-5096(60)90013-2.

Frigo, M., Johnson, S.G., 2005. The design and implementation of FFTW3. Proc. IEEE 93 (2), 216–231. http://dx.doi.org/10.1109/JPROC.2004.840301.

Fuller, K., Roberts, A., 1981. Rubber rolling on rough surfaces. J. Phys. D: Appl. Phys. 14 (2), 221. http://dx.doi.org/10.1088/0022-3727/14/2/015.

Fuller, K., Tabor, D., 1975. The effect of surface roughness on the adhesion of elastic solids. Proc. R. Soc. Lond. Ser. A Math. Phys. Eng. Sci. 345 (1642), 327–342. http://dx.doi.org/10.1098/rspa.1975.0138.

Gao, Y., Bower, A., 2004. A simple technique for avoiding convergence problems in finite element simulations of crack nucleation and growth on cohesive interfaces. Modelling Simulation Mater. Sci. Eng. 12 (3), 453. http://dx.doi.org/10.1088/0965-0393/12/3/007.

Gent, A., 1971. Adhesion of viscoelastic materials to rigid substrates. II. Tensile strength of adhesive joints. J. Polym. Sci. A-2: Polym. Phys. 9 (2), 283–294. http://dx.doi.org/10.1002/pol.1971.160090205.

Gent, A., Petrich, R., 1969. Adhesion of viscoelastic materials to rigid substrates. Proc. R. Soc. Lond. Ser. A Math. Phys. Eng. Sci. 310 (1502), 433–448. http://dx.doi.org/10.1098/rspa.1969.0085.

Gent, A., Schultz, J., 1972. Effect of wetting liquids on the strength of adhesion of viscoelastic material. J. Adhes. 3 (4), 281–294. http://dx.doi.org/10.1080/00218467208072199.

Greenwood, J.A., 2004. The theory of viscoelastic crack propagation and healing. J. Phys. D: Appl. Phys. 37 (18), 2557–2569. http://dx.doi.org/10.1088/0022-3727/37/18/011.

Greenwood, J.A., 2017. Reflections on and extensions of the Fuller and Tabor theory of rough surface adhesion. Tribol. Lett. 65 (4), 1–12. http://dx.doi.org/10.1007/s11249-017-0938-1.

Greenwood, J.A., Johnson, K.L., 1981. The mechanics of adhesion of viscoelastic solids. Philos. Mag. A 43 (3), 697–711. http://dx.doi.org/10.1080/01418618108240402.

Guduru, P.R., 2007. Detachment of a rigid solid from an elastic wavy surface: Theory. J. Mech. Phys. Solids 55 (3), 445–472. http://dx.doi.org/10.1016/j.jmps.2006.09.004.

Guduru, P.R., Bull, C., 2007. Detachment of a rigid solid from an elastic wavy surface: Experiments. J. Mech. Phys. Solids 55 (3), 473–488. http://dx.doi.org/10.1016/j.jmps.2006.09.007.

Jeong, J.-W., Shin, G., Park, S.I., Yu, K.J., Xu, L., Rogers, J.A., 2015. Soft materials in neuroengineering for hard problems in neuroscience. Neuron 86 (1), 175–186. http://dx.doi.org/10.1016/j.neuron.2014.12.035.

Jiang, L., Wu, M., Yu, Q., Shan, Y., Zhang, Y., 2021. Investigations on the adhesive contact behaviors between a viscoelastic stamp and a transferred element in microtransfer printing. Coatings 11 (10), 1201. http://dx.doi.org/10.3390/coatings11101201.

Johnson, K.L., 1985. Contact Mechanics. The press syndicate of the university of cambridge, http://dx.doi.org/10.1017/CBO9781139171731.

Johnson, K.L., 2000. Contact mechanics and adhesion of viscoelastic spheres. In: Microstructure and Microtribology of Polymer Surfaces. ACS Publications, pp. 24–41. http://dx.doi.org/10.1021/bk-2000-0741.ch002.
Johnson, K., Greenwood, J., 2008. A maugis analysis of adhesive line contact. J. Phys. D: Appl. Phys. 41 (15), 155315. http://dx.doi.org/10.1088/0022-3727/41/19/199802.
Johnson, K.L., Greenwood, J.A., Higginson, J.G., 1985. The contact of elastic regular wavy surfaces. Int. J. Mech. Sci. 27 (6), 383–396. http://dx.doi.org/10.1016/0020-7403(85)90029-3.
Johnson, K.L., Kendall, K., Roberts, A.D., 1971. Surface energy and the contact of elastic solids. Proc. R. Soc. Lond. Ser. A 324, 301–313. http://dx.doi.org/10.1098/rspa.1971.0141.
Kesari, H., Doll, J.C., Pruitt, B.L., Cai, W., Lew, A.J., 2010. Role of surface roughness in hysteresis during adhesive elastic contact. Philos. Mag. Philos. Mag. Lett. 90 (12), 891–902. http://dx.doi.org/10.1080/09500839.2010.521204.
Kesari, H., Lew, A.J., 2011. Effective macroscopic adhesive contact behavior induced by small surface roughness. J. Mech. Phys. Solids 59 (12), 2488–2510. http://dx.doi.org/10.1016/j.jmps.2011.07.009.
Landis, C.M., Pardoen, T., Hutchinson, J.W., 2000. Crack velocity dependent toughness in rate dependent materials. Mech. Mater. 32 (11), 663–678. http://dx.doi.org/10.1016/S0167-6636(00)00031-4.
Lin, Y.-Y., Hui, C.Y., 2002. Mechanics of contact and adhesion between viscoelastic spheres: An analysis of hysteresis during loading and unloading. J. Polymer Sci. B 40 (9), 772–793. http://dx.doi.org/10.1002/polb.10140.
Lorenz, B., Krick, B.A., Mulakaluri, N., Smolyakova, M., Dieluweit, S., Sawyer, W.G., Persson, B.N., 2013. Adhesion: Role of bulk viscoelasticity and surface roughness. J. Phys. Condens. Matter 25 (225004), http://dx.doi.org/10.1088/0953-8984/25/22/225004.
Marques, S.C.P., Creus, G.J., 2012. Computational Viscoelasticity. Springer Berlin, Heidelberg, http://dx.doi.org/10.1007/978-3-642-25311-9.
Maugis, D., 1992. Adhesion of spheres: The JKR-DMT transition using a Dugdale model. J. Colloid Interface Sci. 150 (1), 243–269. http://dx.doi.org/10.1016/0021-9797(92)90285-T.
Mazzotta, M.G., Putnam, A.A., North, M.A., Wilker, J.J., 2020. Weak bonds in a biomimetic adhesive enhance toughness and performance. J. Am. Chem. Soc. 142 (10), 4762–4768. http://dx.doi.org/10.1021/jacs.9b13356.
Medina, S., Dini, D., 2014. A numerical model for the deterministic analysis of adhesive rough contacts down to the nano-scale. Int. J. Solids Struct. 51 (14), 2620–2632. http://dx.doi.org/10.1016/j.ijsolstr.2014.03.033.
Müser, Martin H., 2014. Single-asperity contact mechanics with positive and negative work of adhesion: Influence of finite-range interactions and a continuum description for the squeeze-out of wetting fluids. Beilstein J. Nanotechnol. (ISSN: 21904286) 5 (1), 419–437. http://dx.doi.org/10.3762/bjnano.5.50.
Müser, M.H., Persson, B.N., 2022. Crack and pull-off dynamics of adhesive, viscoelastic solids. Europhys. Lett. 137 (3), 36004. http://dx.doi.org/10.1209/0295-5075/ac535.
Neupane, S., Rivas, N.A., Losada-Pérez, P., D'Haen, J., Noei, H., Keller, T., Stierle, A., Rudolph, M., Terfort, A., Bertran, O., et al., 2021. A model study on controlling dealloying corrosion attack by lateral modification of surfactant inhibitors. Npj Mater. Degrad. 5 (1), 1–6. http://dx.doi.org/10.1038/s41529-021-00169-2.
Papangelo, A., Ciavarella, M., 2021a. Adhesion enhancement in a dimpled surface with axisymmetric waviness and rate-dependent work of adhesion. J. Adhes. 1–16. http://dx.doi.org/10.1080/00218464.2021.1944859.
Papangelo, A., Ciavarella, M., 2021b. A criterion for the effective work of adhesion in loading and unloading of adhesive soft solids from rough surfaces. Tribol. Lett. 69 (1), 1–10. http://dx.doi.org/10.1007/s11249-020-01390-x.
Persson, B.N.J., Brener, E.A., 2005. Crack propagation in viscoelastic solids. Phys. Rev. E 71 (3), 1–8. http://dx.doi.org/10.1103/PhysRevE.71.036123.
Persson, B.N., Tosatti, E., 2001. The effect of surface roughness on the adhesion of elastic solids. J. Chem. Phys. 115 (12), 5597–5610. http://dx.doi.org/10.1063/1.1398300.
Popov, V.L., 2021. A note by KL Johnson on the history of the JKR theory. Tribol. Lett. 69 (4), 1–3. http://dx.doi.org/10.1007/s11249-021-01511-0.
Prodanov, N., Dapp, W.B., Müser, M.H., 2014. On the contact area and mean gap of rough, elastic contacts: Dimensional analysis, numerical corrections, and reference data. Tribol. Lett. 53 (2), 433–448. http://dx.doi.org/10.1007/s11249-013-0282.
Störmer, C., 1912. Sur les trajectoires des corpuscules électrisés dans l'espace sous l'action du magnétisme terrestre, avec application aux aurores boréales. Le Radium 9 (11), 395–399. http://dx.doi.org/10.1051/radium:01912009011039501.
Tiwari, A., Dorogin, L., Bennett, A.I., Schulze, K.D., Sawyer, W.G., Tahir, M., Heinrich, G., Persson, B.N.J., 2017. The effect of surface roughness and viscoelasticity on rubber adhesion. Soft Matter 13 (19), 3602–3621. http://dx.doi.org/10.1039/c7sm00177k.
Tiwari, A., Tolpekina, T., van Benthem, H., Gunnewiek, M.K., Persson, B.N.J., 2021. Rubber adhesion and friction: Role of surface energy and contamination films. Front. Mech. Eng. 6, 620233. http://dx.doi.org/10.3389/fmech.2020.620233.
Vaenkatesan, V., Li, Z., Vellinga, W.P., de Jeu, W.H., 2006. Adhesion and friction behaviours of polydimethylsiloxane - A fresh perspective on JKR measurements. Polymer 47 (25), 8317–8325. http://dx.doi.org/10.1016/j.polymer.2006.09.037.
Van Dokkum, J.S., Nicola, L., 2019. Green's function molecular dynamics including viscoelasticity. Modelling Simulation Mater. Sci. Eng. 27 (7), http://dx.doi.org/10.1088/1361-651X/ab3031.
Van Dokkum, J.S., Pérez-Ràfols, F., Dorogin, L., Nicola, L., 2021. On the retraction of an adhesive cylindrical indenter from a viscoelastic substrate. Tribol. Int. 164, 107234. http://dx.doi.org/10.1016/j.triboint.2021.107234.
Violano, G., Afferrante, L., 2019. Adhesion of compliant spheres: An experimental investigation. Proc. Struct. Integr. 24 (2019), 251–258. http://dx.doi.org/10.1016/j.prostr.2020.02.022.
Violano, G., Afferrante, L., 2022a. On the long and short-range adhesive interactions in viscoelastic contacts. Tribol. Lett. 70 (3), 1–5. http://dx.doi.org/10.1007/s11249-022-01611-5.
Violano, G., Afferrante, L., 2022b. Size effects in adhesive contacts of viscoelastic media. Eur. J. Mech. A Solids 104665. http://dx.doi.org/10.1016/j.euromechsol.2022.104665.
Violano, G., Chateauminois, A., Afferrante, L., 2021a. A JKR-like solution for viscoelastic adhesive contacts. Front. Mech. Eng. 7, 25. http://dx.doi.org/10.3389/fmech.2021.664486.
Violano, G., Chateauminois, A., Afferrante, L., 2021b. Rate-dependent adhesion of viscoelastic contacts. Part I: Contact area and contact line velocity within model randomly rough surfaces. Mech. Mater. 160, 103926. http://dx.doi.org/10.1016/j.mechmat.2021.103926.
Violano, G., Chateauminois, A., Afferrante, L., 2021c. Rate-dependent adhesion of viscoelastic contacts. Part II: Numerical model and hysteresis dissipation. Mech. Mater. 158, 103884. http://dx.doi.org/10.1016/j.mechmat.2021.103884.
Violano, G., Orlando, G., Demelio, G., Afferrante, L., 2022. Adhesion of viscoelastic media: An assessment of a recent JKR-like solution. IOP Conf. Ser.: Mater. Sci. Eng. 1214, 012038. http://dx.doi.org/10.1088/1757-899x/1214/1/012038.
Wang, A., Zhou, Y., Müser, M.H., 2021. Modeling adhesive hysteresis. Lubricants 9 (2), 17. http://dx.doi.org/10.3390/lubricants9020017.
Waters, J.F., Guduru, P.R., 2010. Mode-mixity-dependent adhesive contact of a sphere on a plane surface. Proc. Royal Soc. A 466 (2117), 1303–1325. http://dx.doi.org/10.1098/rspa.2009.0461.
Waters, J.F., Lee, S., Guduru, P.R., 2009. Mechanics of axisymmetric wavy surface adhesion: JKR-DMT transition solution. Int. J. Solids Struct. 46 (5), 1033–1042. http://dx.doi.org/10.1016/j.ijsolstr.2008.10.013-z.
Zhu, Y., Zheng, Z., Zhang, Y., Wu, H., Yu, J., 2021. Adhesion of elastic wavy surfaces: Interface strengthening/weakening and mode transition mechanisms. J. Mech. Phys. Solids 151, 104402. http://dx.doi.org/10.1016/j.jmps.2021.104402.